International Journal of Hydrogen Energy 158 (2025) 150309

Contents lists available at ScienceDirect

International Journal of Hydrogen Energy

journal homepage: www.elsevier.com/locate/he

Accounting for meteorological and load data uncertainty in the optimal design of off-grid hybrid renewable energy systems

Florent Struyven [a], Mathieu Sellier [b], Myeongsub Kim [c], Rosalinda Inguanta [d], Farkad A. Lattieff [e], Philippe Mandin [a,*]

[a] Institut de Recherche Dupuy de Lôme, UMR CNRS 6027, Lorient, France
[b] Department of Mechanical Engineering, University of Canterbury, Christchurch 8140, New Zealand
[c] Department of Ocean and Mechanical Engineering, Department of Biomedical Engineering, Florida Atlantic University, Boca Raton, USA
[d] Department of Engineering, University of Palermo, Palermo, Italy
[e] College of Engineering, University of Baghdad, Baghdad, Iraq

ARTICLE INFO

Keywords:
Microgrids
HRES
Hydrogen
MOEA

ABSTRACT

This study presents a methodological contribution to the optimal design of an off-grid hybrid renewable energy systems (HRES) producing both electricity and drinking water. Beyond simulating the operation of a system combining solar photovoltaic and wind generation with battery and hydrogen storage , the work focuses on a critical yet often overlooked issue: the uncertainty associated with meteorological and consumption input data. A multi-objective optimization model, implemented in Julia, is used to determine system configurations that minimize the cost of energy and water while maximizing the share of renewable energy. The analysis demonstrates that the selection of input data has a significant influence on system design results. A methodology is proposed to identify the most favorable and most unfavorable input datasets. A novel shortage indicator is introduced to quantify energy deficits during periods when renewable production is insufficient to meet demand. This indicator enables interpretation of the underlying causes of cost and sizing variations, by linking them to storage requirements. The methodology is applied to the island of Molène (France) using meteorological and consumption data from 2018 to 2023. The results highlight the strong sensitivity of system design to input variability, and provide a framework for robust analysis and planning under uncertainty.

1. Introduction

Today, diesel generation remains the most popular solution for producing electricity and, indirectly, drinking water in areas with little or no connection to the grid. Over 10,000 islands worldwide, home to around 750 million people, still depend on diesel generators to supply electricity and drinking water via water purification systems. Those with populations of between 1,000 and 100,000 devote a significant proportion of their gross domestic product to fuel imports [1].

However, the use of diesel generators in remote locations has environmental drawbacks, and operating costs can be high due to fuel transport and logistical problems [1–3]. The cost of energy produced by diesel generators depends essentially on the cost of fuel, which can vary significantly depending on international geopolitical context. These fluctuations can lead to high energy costs and pose supply risks [4–6]. In the past, predictions concerning the evolution of these costs have mostly turned out to be wrong, but the trend suggests a likely increase in fuel prices [7,8].

Network connections, when possible, require the establishment of costly and invasive infrastructure, and the areas concerned may suffer from network stability problems due to their remoteness [9]. Since the legally binding global climate change treaty signed in Paris during the international climate summit (COP21) on 12 December 2015, the world has been striving to limit its greenhouse gas emissions, although some countries have withdrawn from these agreements [10–12]. The use of diesel generators and excessive expenditure to connect sites to networks whose energy is mainly produced by fossil fuels can only drive the world further away from respecting these agreements.

Renewable energy sources such as wind and solar power are widely recognized as essential to tackling these challenges [13]. They also offer the most appropriate and cost-effective solution for populations in developing regions [1].

The cost of renewable energy technologies, such as photovoltaic solar power, is already competitive or even lower than—that of fossil

* Correspondence to: Centre de Recherche C. HUYGENS, Rue de Saint-Maudé – BP 92116, F-56321 Lorient Cedex, France.
E-mail address: philippe.mandin@univ-ubs.fr (P. Mandin).

https://doi.org/10.1016/j.ijhydene.2025.150309
Received 31 March 2025; Received in revised form 10 June 2025; Accepted 2 July 2025
Available online 21 July 2025

Nomenclature

Abbreviations

AT	Annual Throughput
BESS	Battery Energy Storage System
BT1	Battery bank 1
BT2	Battery bank 2
C3POe	Plug & Play Water-Electricity Sustainable Coupling System for Islands and Isolated Coastal Sites
CONV,X	Electrical converter assigned to the subsystem "X"
CTF	Cycle To Failure
CURT	Curtailment
DOD	Depth Of Discharge
EL	Electrolyzer
EWMS	Energy & Water Management System
EXT	External sources of energy
FC	Fuel Cell
H2	Dihydrogen
HRES	Hybrid Renewable Energy System
IO	On–Offs
LB	Lower Boundary
LOH	Level Of Hydrogen
LOW1	Level Of drinkable Water
LOW2	Level Of pure Water
PR	Project
pv	Photovoltaïc
RES	Renewable Energy Sources
RO1	Reverse Osmosys System producing drinkable water
RO2	Reverse Osmosys System producing pure water
SOC	State Of Charge
UB	Upper Boundary
wt	Windturbine

Objective

$\frac{E_{EXT}}{E_{Load}}$	Ratio between energy from a source external to the system and energy consumed by system users
COEW	Cost Of Energy& Water [€·kWh^{-1}]

Parameters

η_X	Efficiency of subsystem "X" $[0-1]$
Cp_X	Capacity of the subsystem "X"
$k_{mix,pv}$	Ratio between the energy produced by photovoltaic panels and the energy produced by all RES during one year $[0-1]$
k_{power}	Ratio of energy produced by RES to energy consumed during one year $1,\ldots,3.5$
$P_{X,rated}$	Rated power of the subsystem "X" [W]
LT	Lifetime throughput [kWh]

Variables

$\dot{m}_{H2}(t)$	Average quantity of dihydrogen produced or consumed by subsystem "X" for one hour at time t [kg h^{-1}]
$IO_X(t)$	Operating status of subsystem "X" at time t $ON->0$ *or* $OFF->1$
L_X	Lifetime of subsystem "X" [years]
$P_X(t)$	Average power delivered or consumed by subsystem "X" for one hour at time t [W]
$Q_X(t)$	Average water flow delivered or consumed by subsystem "X" for one hour at time t [m^3 h^{-1}]
t	Simulation time [h]

fuels. Between 2010 and 2019, the costs of solar panels, onshore wind turbines, and offshore wind turbines decreased by 82%, 40%, and 29%, respectively, with further reductions anticipated in the coming years [13]. In this context, renewable energy-based systems for supplying electricity and water to off-grid or remote locations are becoming increasingly relevant. However, the intermittency of renewable energy generation remains a major barrier to its large-scale deployment and must be addressed through effective energy storage solutions and robust energy management strategies.

To ensure a stable electricity supply for off-grid systems and continuously meet demand, storage systems must be capable of buffering renewable energy fluctuations—storing excess energy when generation exceeds demand and supplying energy when production falls short [14,15]. Each storage technology has specific limitations, and its applicability largely depends on the temporal scale of the fluctuations. Solutions designed to handle rapid variations over milliseconds differ significantly from those required for managing seasonal storage needs. When renewable sources represent more than 80% of the energy mix, long-duration energy storage becomes critical for minimizing the overall system cost [16].

The cost of renewable energy technologies, such as photovoltaic solar power, is now competitive with — or even lower than — that of fossil fuels. From 2010 to 2019, the costs of solar panels, onshore wind turbines, and offshore wind turbines declined by 82%, 40%, and 29%, respectively, and are expected to continue decreasing [13]. In this context, renewable-based systems for supplying electricity and water to off-grid or remote areas are becoming increasingly attractive. Nevertheless, the intermittency of renewable energy production remains a major barrier to large-scale deployment and must be mitigated through efficient energy storage and advanced energy management strategies.

To maintain a stable power supply in off-grid systems and meet continuous demand, storage technologies must buffer fluctuations in renewable generation—by storing surplus energy when production exceeds demand and discharging it when production is insufficient [14,15]. Each storage option has inherent limitations, and its suitability depends primarily on the time scale of variability. Technologies designed to address rapid, sub-second fluctuations differ significantly from those intended for seasonal storage. When renewable sources account for over 80% of the energy mix, long-duration storage becomes essential to minimizing overall system costs [16].

Batteries are ideal for small-scale, short-term energy storage due to their enhanced performance and decreasing costs, making lithium-ion and lead–acid batteries the preferred choice for integrating local renewable energy sources into national grids. However, for longer-term storage applications, such as achieving energy self-sufficiency for isolated sites disconnected from the grid, batteries become cost-prohibitive, and hybrid solutions incorporating other storage technologies are more practical and economical [9]. Power-to-gas technologies, and power-to-hydrogen in particular, offer several advantages including high energy density, grid stabilization services, negligible self-discharge losses, flexibility in relation to site topography, and

environmental benefits through reduced local pollutants and CO2 emissions. These technologies are positioned to play a key role in long-term, large-scale energy storage, particularly given the growing adoption of renewable energy sources [17]. Hydrogen production through water electrolysis represents a promising long-term storage solution for isolated microgrids since it can prevent battery oversizing [4]. One of the main barriers to electrolysis-based hydrogen adoption is its cost compared to alternatives based on fossil feedstocks.

Global hydrogen demand is estimated at 80 million tonnes per year and is predominantly met by hydrogen produced from fossil fuels using methods such as steam methane reforming [18]. However, a favorable regulatory environment, increased investment in the hydrogen sector, and the resulting research projects should enable the electrolysis process to improve its performance over the next few years [19,20].

Hybrid renewable energy systems (HRES), i.e., the combination of hydrogen and batteries for energy storage, have been extensively studied in the literature, demonstrating significant potential for delivering reliable and sustainable power supplies to customers [21]. Storage systems need to be sized to meet instantaneous power requirements. One of the major disadvantages of batteries is that their power output is coupled to their storage capacity, which generally leads to single-battery systems being oversized to address periods of energy shortage throughout the year. Frequent operational changes in fuel cells and electrolyzers must be minimized to avoid performance degradation and extend their lifespan. Batteries can absorb short-term variations, thereby reducing the variability of renewable energy production. To protect batteries and avoid shortening their lifespan, it is essential to avoid overcharging and overdischarging, which can be mitigated by using complementary storage technologies such as hydrogen [22].

The study presented in this article is part of the C3POe (Plug & Play Water-Electricity Sustainable Coupling for Islands and Isolated Coastal Sites). The objective of the C3POe project is to design a system capable of meeting the water and electricity needs of isolated populations in a sustainable and holistic manner, using renewable resources to minimize the system's environmental impact. The system must be modular to adapt to changing needs, and easy to transport and maintain.

The system will be installed primarily on Brittany islands not connected to the French national grid: Ouessant, Sein, Molène, and Chausey. The French Energy Regulatory Commission, the independent authority responsible for guaranteeing the smooth operation of French energy markets for the benefit of consumers, has reported an electricity production cost of 0.455 € kWh^{-1} for these islands (which is approximately double the average price per kWh paid in mainland France), and an electricity production mix based predominantly on fossil fuels, with 94.7% fossil fuels and 5.3% photovoltaic energy.

The risk of drinking water shortages on these islands is also a critical factor to consider. These islands have been and continue to be exposed to water shortages due to a combination of drought, physical limitations, and anthropogenic pressure on water resources. Seawater desalination technologies represent the most competitive solution, compared to transporting water by boat or connecting to the mainland network [23].

A diagram of the C3POe system is shown in Fig. 1. The system consists of electrical, water, and hydrogen networks and is powered by a mix of energy from wind turbines and photovoltaic solar panels. The subsystems are connected to an alternating current (AC) bus via electrical converters. When the system is unable to supply the energy required by users, it can utilize a non-renewable energy source external to the system. The energy produced by the system is used to meet users' electricity and water requirements. In the event of overproduction from renewable energy sources, some of this energy is curtailed. The system can store the energy generated by renewable sources in a battery energy storage system (BESS) or in a Power to Power (P2P) chain that transforms electricity into hydrogen. The hydrogen chain comprises an electrolyzer, a hydrogen tank, and a fuel cell. Water is produced by two reverse osmosis systems. The first, RO1, produces drinking water from seawater, while the second, RO2, produces pure water from drinking water for the electrolyzer. All these subsystems are controlled by an energy and water management system (EWMS), which determines whether they are switched on or off, and their operating modes.

Grid-isolated microgrid systems like the C3POe system face the challenge of reconciling conflicting objectives:

- ensuring high power and water reliability;
- minimizing energy and water costs;
- reducing carbon emissions.

To find cost-effective solutions capable of continuously adjusting their operation to the fluctuating output of renewable sources, it is often necessary to combine several power generators and storage systems, which increases the complexity of their design and sizing [24,25].

The principle of a hybrid system is to combine the advantages of different storage technologies in an attempt to:

- achieve the best efficiency;
- obtain a sufficiently large storage capacity to cover periods of energy production shortages throughout the year;
- minimize maintenance and component replacement over the lifetime of the project.

Efficiency is crucial in energy storage, as lower efficiency means that either additional generation capacity will be required to meet demand, or extra storage capacity will be needed to ensure system requirements are met. The efficiency of an isolated microgrid system depends on the efficiency of each of its subsystems, but primarily on the proportion of energy from renewable sources that can be redistributed to consumers. Energy from renewable sources can either be distributed directly to consumers, stored by the system for later redistribution, or lost when the system's capacity to store surplus energy is exceeded. Despite this, the system may find itself unable to meet consumer needs, in which case a source external to the system must be used. The main challenge in sizing a microgrid system based on renewable energy is to minimize the proportion of energy from an external source used to meet consumer needs, while simultaneously minimizing the system cost. To increase the system's capacity to absorb and return energy from renewables, its cost must be increased. Conversely, decreasing this capacity means increasing the proportion of energy from external sources that must be used to meet consumer demand. A sizing study must assess the extent to which these two objectives conflict, in order to provide project investors with a decision-making criterion.

Another critical objective is to reduce greenhouse gas emissions, which are directly linked to the share of fossil fuels in the energy mix. In the case of islands and isolated sites where existing electricity production is predominantly fossil-based, reducing the share of energy coming from outside the HRES system helps to reduce greenhouse gas emissions. Apart from the proportion of external energy used, the emissions generated by the HRES system are essentially due to the emissions produced during the construction of its various components.

The use of commercial software provides the computational framework needed to simulate the operation of off-grid systems. However, this approach can constrain system modeling and limit understanding of the methods employed. A specific energy distribution strategy is employed, which may not be appropriate for the system under study. From a general perspective, the sizing methodology and objectives may differ from what is desired by users. This is why there are many publications developing their own methodologies [3,5,6,21,26–30].

The first step in the sizing and optimization process of off-grid HRESs is to provide an accurate model capable of estimating the cost of producing water and electricity over the lifetime of the project. This results in a large number of decision variables when analyzing this type of complex system.

Several model design choices can affect the final result. The first challenge is to obtain a set of input data that reflects the weather and

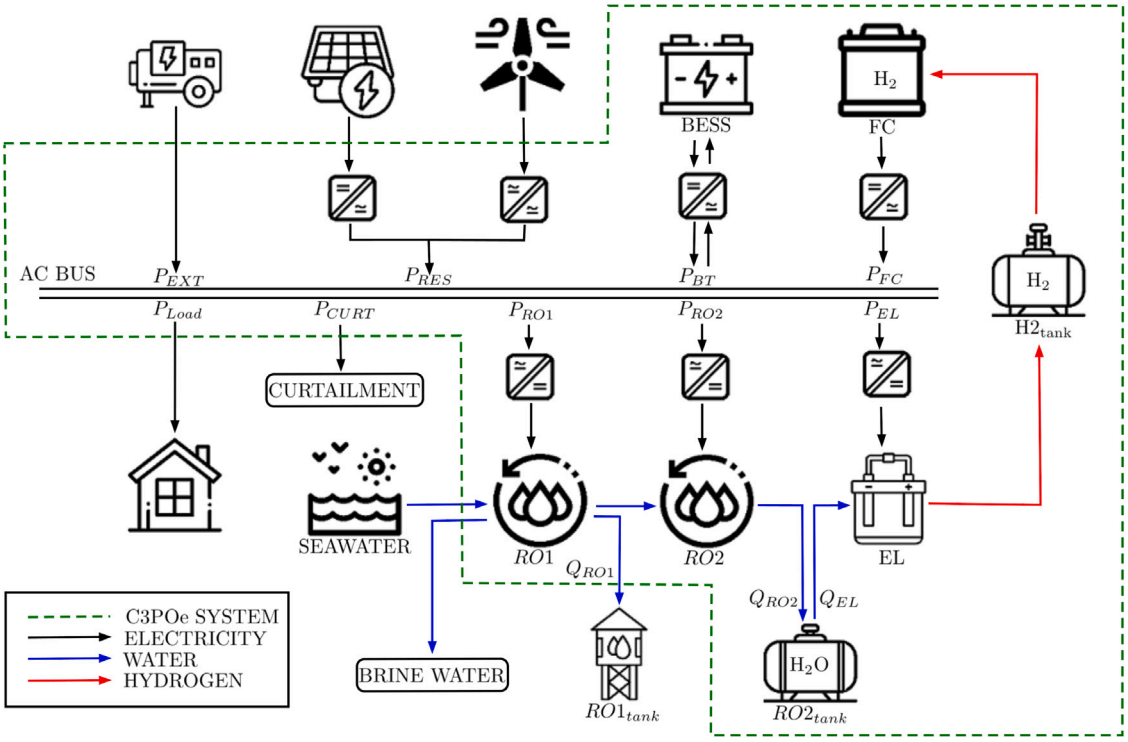

Fig. 1. Schematic diagram of the C3POe system, with connection of the various sub-systems to the water, electricity and hydrogen networks. The subsystems controlled by the EWMS supply or draw power P_X from the AC electric bus. AC BUS: Alternative Current bus, BESS: Battery Energy Storage Systems, EL: Electrolyzer, FC: Fuel Cell, RO1: Reverse Osmosys system producing drinking water from seawater, RO2: Reverse Osmosys system producing pure water for electrolysis of drinking water, $RO1_{tank}$: drinking water tank, $RO2_{tank}$: pure water tank.

consumption conditions at the specific site, on the assumption that this set of past data describes future conditions at the site.

A common approach in the literature is to rely on typical single-year meteorological and demand data and assume that this data is repeated from one year to the next over the life of the project. Mandelli et al. tested the effect of load profile uncertainty on the sizing of PV-battery systems [31]. They found that testing several load profiles led to a more robust system sizing that responded reliably to different input data. Javed et al. conducted a study assessing the impact of interannual renewable energy production variability on the optimal configuration of an off-grid renewable energy system, employing four decades of meteorological and load demand data [27]. With their model, they found that using a range of data over six years considerably reduced uncertainties, and resulted in an operating cost around 35% higher than a simulation based on a single year. This is because energy storage requirements are more sensitive to the length of the simulation period, and often increase with longer periods.

The time step of the input data influences the choices and simplifications made to model the behavior of the various system components, such as the electrolyzer and fuel cell. The influence of the time step and the resulting assumptions on HRES sizing is a parameter that has received little attention in the literature [32,33]. For a time step greater than or equal to an hour, the influence of the start-up and shutdown times of electrolyzers and fuel cells can be neglected. As a general rule, the performance of the various system components is averaged over the duration of the time step.

The sizing and technical and economic study of these systems cannot be carried out without incorporating an energy management strategy [34]. The energy efficiency of the whole system and the total operation time that each technology integrated into the system undergoes will depend on the management rules put in place [35–37].

The lifespan of the various subsystems also needs to be taken into account, as their performance degrades over the life of the project and they need to be replaced, increasing the system cost each time they are replaced. Very few studies include component replacement, yet the impact of component replacement costs is non-negligible [9]. Once the model has been established, the system parameters are sized by minimizing one or more objective functions using an optimization algorithm. The relationship between the objective function and system parameters is often non-linear and complex. The main objectives studied are power supply reliability, optimized operating costs, reduced environmental impact, and demand management, among others. Saharia et al. reviewed the different objective functions and algorithms used to dimension HRES, focusing on methodologies based on genetic algorithms and particle swarm optimization [38].

Salehi et al. carried out a review of single-objective and multi-objective optimization methods to size HRES for [39]. The most popular approaches are based on the analysis of Pareto fronts obtained from multi-objective evolutionary algorithms, which give better results in terms of computational effort, robustness, faster convergence, and ability to handle multiple conflicting objectives.

A simplified diagram of the numerical model created is shown in Fig. 2. It is subdivided into a performance model, an ageing and degradation model, and an economic model.

The study presented in this article aims to determine the size of the main components of this system to best meet the water and electricity needs of an island community. The article focuses on the specific study of the island of Molène, analyzing the technical solution proposed for this site. A techno-economic analysis was carried out after defining a sizing methodology and a reference strategy for energy management. The assessment is based on data and technical information provided by the various project stakeholders.

Unlike many other studies, photovoltaic and wind power systems are not sized. The choice of the type and power of renewable energy production systems to be installed will depend on topological, environmental, administrative, and political factors, among others, which are beyond the scope of this study. As a result, several renewable energy production mix scenarios have been studied. The search for an optimal

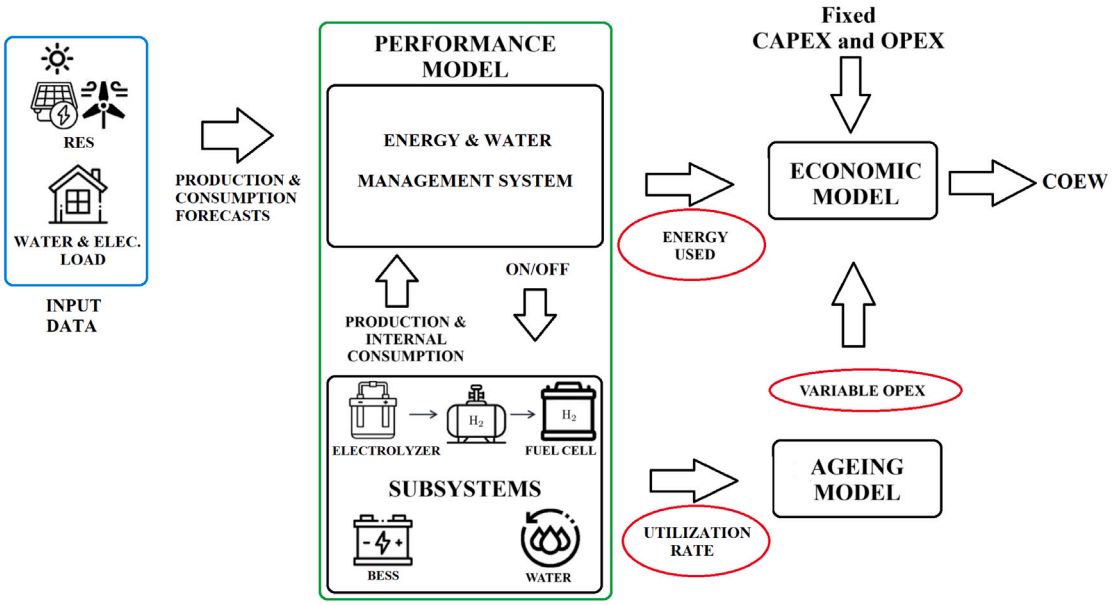

Fig. 2. Simplified diagram of the model used to determine the cost of the energy and water produced. Input data, consisting of user electricity and water consumption and energy generated by renewable sources (RES), are determined hour by hour over the course of a year, enabling the performance model to calculate the energy stored, consumed, or delivered to the consumer by the various subsystems, as well as their utilization rates. This enables the aging model to calculate variable system operating costs (variable OPEX). Based on this information, the economic model calculates the cost of energy and water over the life of the project.

Pareto front is carried out for each of these scenarios. One of the distinguishing features of this study is that it presents a set of rules for simulating the behavior of a management system that will control the electricity, hydrogen, and water networks simultaneously. Indeed, the originality of the proposed approach is to produce pure water for the electrolysis needs from renewable energy production, so there is a strong coupling between the pure water level and the hydrogen level. The decision was made to take into account the performance degradation and lifetime of the electrolyzer, fuel cells, and batteries, as they play a significant role in the total cost of the project, which is rarely discussed in this type of publication.

Most HRES design studies rely on techno-economic optimization models using a single year of meteorological and load data, typically assumed to be representative of long-term conditions. However, this assumption overlooks the inherent variability and uncertainty of renewable resources and energy demand, particularly in isolated or off-grid contexts. Recent works, such as those by Javed et al. and Oyewole et al. use multi-annual datasets, demonstrating that inter-annual variability can significantly affect design outcomes [27,40]. Despite these efforts, few studies have proposed a systematic methodology to quantify this uncertainty and to identify its underlying causes.

In the present study, this gap is addressed through the development of a methodological framework capable of identifying the most favorable and unfavorable input years from a system design perspective, based on their influence on key techno-economic indicators such as the cost of energy. In addition, a shortage indicator is introduced to characterize the periods during which energy production falls short of demand, thereby revealing the storage requirements that explain variations in system performance and cost. This contribution provides a novel basis for evaluating the sensitivity of HRES design to input data uncertainty and offers a useful tool for more robust and resilient system planning.

The structure of this paper is as follows: in Section 2 the different scenarios based on meteorological and consumption data are presented; in Section 3 the equations and the energy and water management system of the model are explained; in Section 4 the objective functions and the optimization algorithm used are specified, and the results are shown in Section 5.

2. Scenario inputs

For the purposes of the simulation, several scenarios have been created based on consumption and weather data for the years 2018 to 2023, i.e. six years as recommended by Javed et al. [27]. Another reason for choosing 6 years is that consumption data are only available for the years 2017 to 2023. Meteorological data were obtained from the Photovoltaic Geographical Information System (PVGIS) developed by the European Commission's Joint Research Center. The application provides hour-by-hour access over a typical year (2005–2020) for a given latitude and longitude, to average temperature, humidity and irradiance data, as well as wind speed, wind direction and atmospheric pressure, all of which are needed to calculate the power generated by a solar photovoltaic panel or a wind turbine. The PVGIS model was used to obtain the power generated by crystalline silicon 1 kW-peak solar panel $P_{RES,pv,1kWp}$ as shown in Fig. 3. The default value of 14% for the overall losses has been kept. The panels are assumed to be fixed and the slope and the azimuth are optimized by PVIGS. The wind power module of the National Renewable Energy Laboratory's PySAM Python library was used with data from PVGIS to determine the power produced by wind turbines $P_{RES,pv,26kW}$ as shown in Fig. 4 [41]. The characteristics of a 26 kW wind turbine were used. The power delivered by the turbine as a function of wind speed is shown in Fig. 5. This type of 26 kW wind turbine is well suited to the Brittany islands, as it has already been installed on other islands in the region (Saint-Nicolas and Penfret islands in the Glénan Archipelago).

A profile of hourly electricity consumption on the island of Molène has been drawn up from data made available by the public authorities for each year of the study interval. Electricity consumption data for the island of Molène are not available. However, data from the nearest town, Brest, are available on the ODRé website (Open Data Réseaux Énergies). Molène has a population of around 200. The consumption profile of the city of Brest $P_{Load,elec,Brest}(t)$ is scaled to correspond to an average electricity consumption of 200 inhabitants (2400 kWh per inhabitant per year), i.e. 480 MWh per year, as shown in Eq. (1).

$$P_{\text{Load, elec, Molène}}(t) = P_{\text{Load, elec, Brest}}(t) \times \frac{480\ [\text{MWh}]}{\sum_{t=1}^{8760} P_{\text{Load, elec, Brest}}(t)} \quad (1)$$

In other words, the electricity consumption profile of Molène $P_{\text{Load, elec, Molène}}(t)$ is different from one year to the next because it

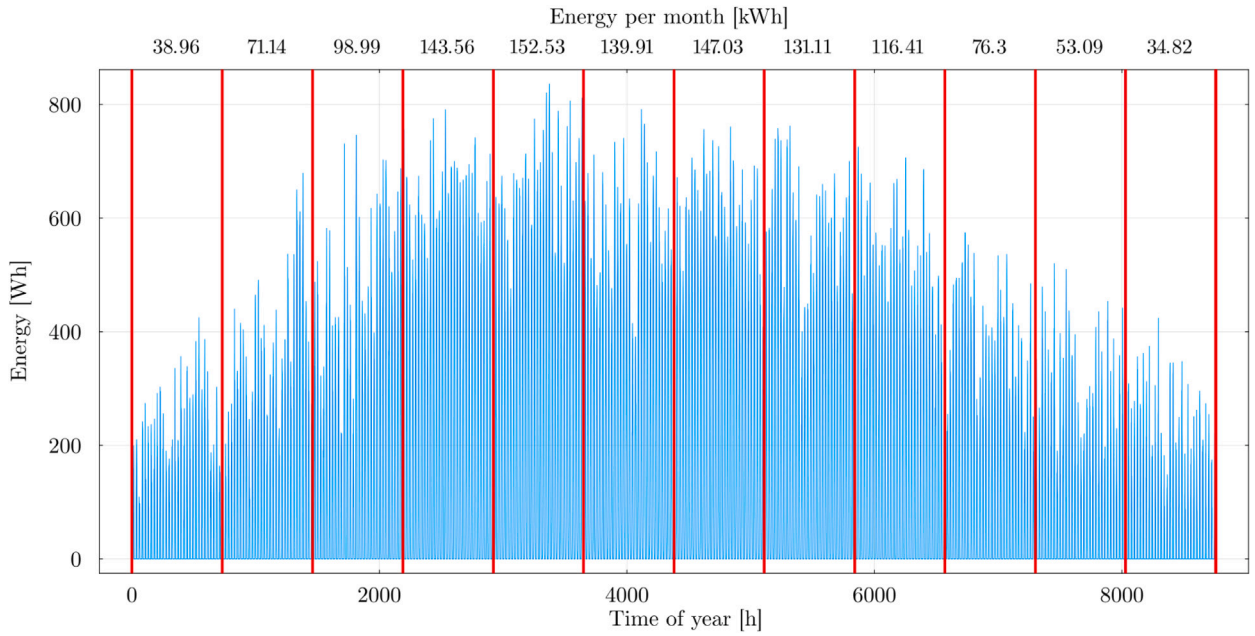

Fig. 3. Photovoltaic power profile $P_{RES,pv,1\text{kW}p}$. Annual energy production in [Wh] of crystalline silicon 1 kWp solar panel located on the island of Molène given hour by hour. For this graph, the photovoltaic energy produced each hour of the year has been averaged from the results provided by PVGIS for the years 2018–2023. The default value of 14%, recommended by PVGIS developers for the overall losses has been kept. The panels are assumed to be fixed and the slope and the azimuth are optimized by PVGIS.

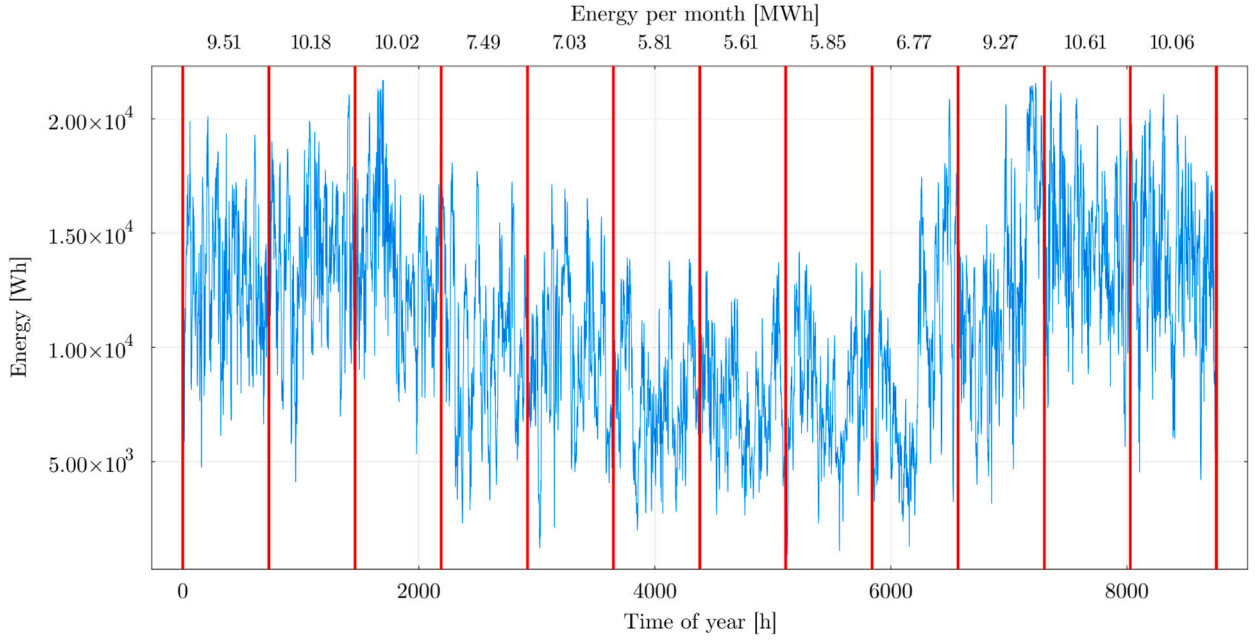

Fig. 4. Wind turbine power profile $P_{RES,pv,26\text{kW}}$. Annual energy production in [Wh] of a 26 kW rated wind turbines located on the island of Molène given hour by hour. The power versus wind speed curve used to obtain these results is shown in Fig. 5. For this graph, the energy produced by the wind turbine each hour of the year has been averaged from the results provided by PYSAM's windpower module with weather data extracted from the PVGIS database for the years 2018–2023.

corresponds to the profile of Brest's inhabitants, but the energy consumed per year remains constant at 480 MWh. Hour-by-hour user water consumption data are not available. However, since drinking water storage is often available and not very restrictive, it can be assumed that variations in water consumption can be cushioned by such storage. Accordingly, water consumption was evenly distributed throughout the year. A base of 150 liters of water consumed per day per inhabitant was taken, which corresponds to the national average. To account for the impact of water consumption on electricity consumption, the production capacity of the reverse osmosis system in m^3 of water produced per kWh consumed was used, which corresponds to an annual electricity consumption of 65 MWh.

Combining the electricity consumption of residents with the electrical requirements of the reverse osmosis system to produce drinking water, a global hour-by-hour electricity consumption profile P_{Load} throughout the year is established for each year. An average profile is shown in Fig. 6.

Several renewable energy production scenarios are proposed. To facilitate reasoning on the impact of renewable energy production on system sizing, the energy produced by a 26 kW wind turbine and a

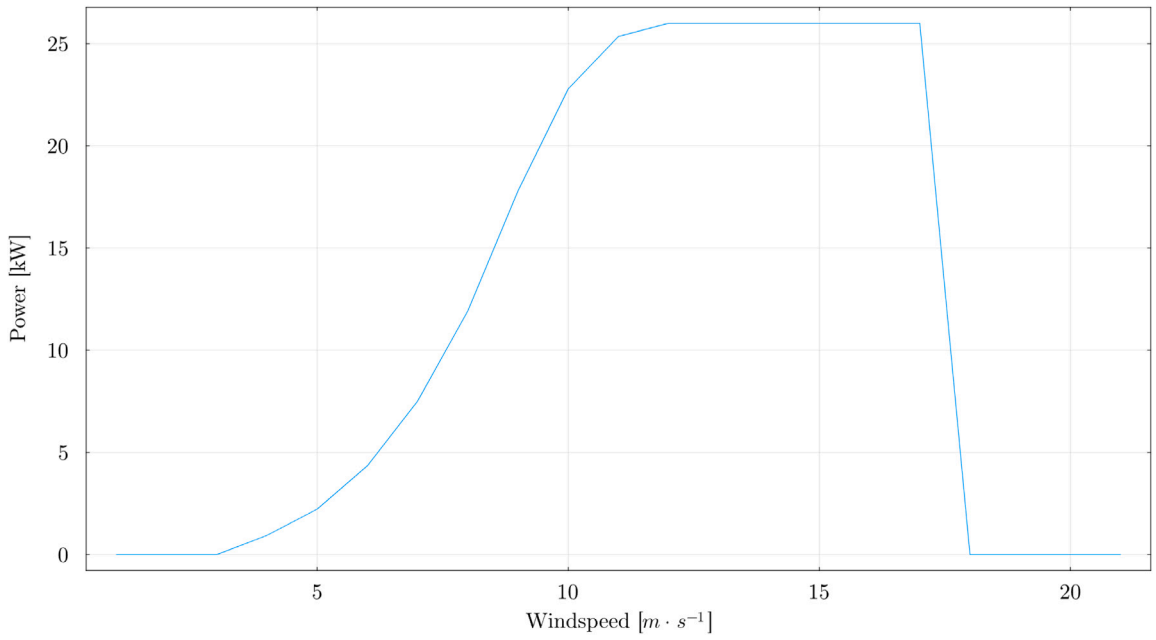

Fig. 5. Power versus wind curve for the 26 kW wind turbine.

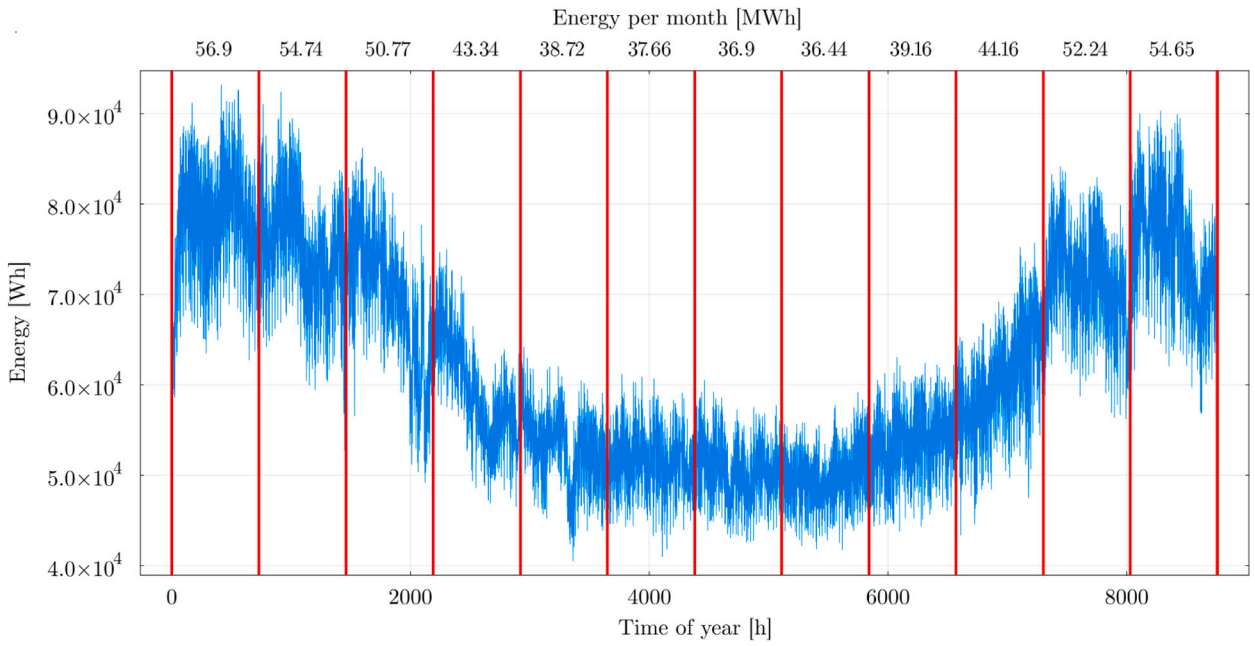

Fig. 6. Cumulative profile $P_{Load}(t)$ $(t : 0 \longmapsto 8760)$ of user electricity consumption and equivalent electricity consumption for typical hourly water production over one year on the island of Molène. Annual energy consumption in [Wh] given hour by hour and sum of energy consumed per month in [MWh].

Table 1
Assumptions for annual energy consumption and production on Molène Island expressed in MWh as a function of the factor k_{power}.

k_{power}	$\sum_{t=1}^{8760} P_{RES}(t)$ [MWh]	$\sum_{t=1}^{8760} P_{Load}(t)$ [MWh]
1	545	
1.5	817,5	
2	1090	
2.5	1362,5	$480 + 65 = 545$
3	1635	
3.5	1907,5	

1 kWp solar panel are scaled so that the sum of annual renewable energy production corresponds to the sum of electricity consumption P_{Load} multiplied by a factor k_{power}. A second parameter $k_{mix,pv}$ with values between 0 and 1 giving the share of energy produced by solar photovoltaic panels in the mix is introduced.

The sum of the energy produced by photovoltaic panels $P_{RES,pv}$ and wind turbines $P_{RES,wt}$ for each scenario satisfies with the following equations:

$$\sum_{t=1}^{8760} P_{RES,pv}(t) = k_{mix,pv} k_{power} \sum_{t=1}^{8760} P_{Load}(t) = n_{pv} \sum_{t=1}^{8760} P_{RES,pv,1kWp}(t) \qquad (2)$$

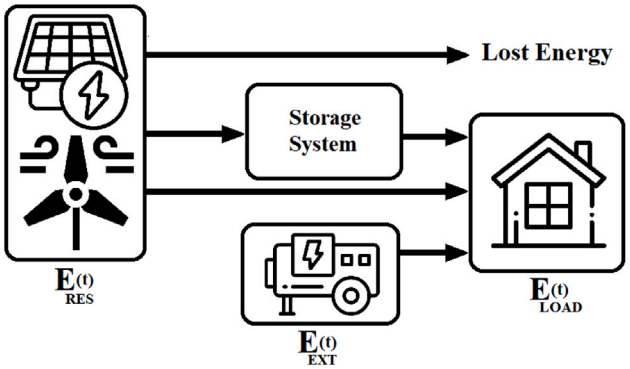

Fig. 7. Diagram of a simplified distribution of the energy produced by renewable sources $E_{RES}(t)$ and the distribution of the energy consumed by users $E_{Load}(t)$. Despite the existence of buffer storage to compensate for the intermittency of $E_{RES}(t)$, part of the energy is lost, and in order to meet the needs of consumers at all times, it is sometimes necessary to call on an energy source external to the system $E_{EXT}(t)$.

$$\sum_{t=1}^{8760} P_{RES,wt}(t) = (1.0 - k_{mix,pv}) k_{power} \sum_{t=1}^{8760} P_{Load}(t) = n_{wt} \sum_{t=1}^{8760} P_{RES,pv,26kW}(t) \tag{3}$$

$$\sum_{t=1}^{8760} P_{RES}(t) = k_{power} \sum_{t=1}^{8760} P_{Load}(t) = k_{power} \times 545[\text{MWh}] \tag{4}$$

where P_{RES} is the cumulative power generated by nb_{wt} 26 kW wind turbines and nb_{pv} kWp solar photovoltaic panels. The Table 1 shows annual energy consumption and production as a function of parameter k_{power}. This scaling is made possible because, firstly, the PVGIS model is linear, i.e., the energy supplied by the solar panel is proportional to the installed power, and secondly, it is assumed that the wind turbines installed do not interfere with each other. In reality, the wind turbines in a wind farm disturb each other according to wind direction and the position of each within the wind farm, as simulated in PySAM's wind turbine module. However, for the sake of simplicity, the wind turbine module has been used with the input parameter of a wind farm with a single wind turbine.

The scaling of energy production data for renewables is a key aspect of this study. In fact, each year of the project's lifespan, once installed, renewables will produce a different amount of energy depending on weather conditions. In the same way, user consumption will differ from year to year. As a result, the cost of the energy produced by the system will depend on the evolution of weather conditions and the needs of system users over the life of the project. To account for this variability in energy prices, the combination of the worst and best consumption and weather conditions has been selected for each scenario, based on past data from the years 2018 to 2023. To calculate the cost of energy, the model reuses the same input data for each year of the project's lifetime. This approach produces a likely range of low and high energy costs, depending on the scenario studied.

A shortage indicator has been defined to assess the suitability of each year's data set for each scenario. This indicator is based on a simplified energy management system. It can be interpreted as a means of assessing the mismatch between renewable energy production and consumption. As shown in Fig. 7, renewable energy production $E_{RES}(t)$ is intermittent, so some of it can be distributed directly to the user, stored inside a storage system, or lost. As users' energy consumption $E_{Load}(t)$ is difficult to predict, in order to meet their needs on a permanent basis, the energy has to be provided either directly from the RES, or from the storage system, or from an external source $E_{EXT}(t)$. Assuming that the storage system is perfect (i.e., operating without losses, but also being able to store and redistribute an unlimited amount of energy), the shortage indicator can be used to determine how much energy needs to be stored in order to be able to continuously meet users' energy requirements for one year without recourse to an external source.

At each time step, when $\left(P_{Load}(t) - P_{RES}(t)\right) < 0$, renewable energy sources meet all consumer needs and the surplus is stored. When $\left(P_{Load}(t) - P_{RES}(t)\right) > 0$, the renewable energy sources only meet part of the consumers' needs and the difference is taken from storage. The system begins to be in shortage when $P_{Load}\left(t_{start\ shortage}\right) > P_{RES}\left(t_{start\ shortage}\right)$. The system exits the shortage when $\sum_{t=t_{start\ shortage}}^{t_{equilibrium}} \left(P_{Load}(t) - P_{RES}(t)\right) \Delta t \geq 0$. Between the time $t_{start\ shortage}$ when the shortage begins and the time $t_{equilibrium}$ when the system returns to equilibrium, the maximum energy deficit reached makes it possible to determine the amount of energy to be stored $E_{shortage}$ before the shortage to be able to meet users' needs during this period.

$$\begin{aligned} E_{shortage} = Maximum \Bigg[& \left(P_{Load}(t_{start\ shortage}) - P_{RES}(t_{start\ shortage})\right) \Delta t \\ & , \ldots , \sum_{t=t_{start\ shortage}}^{t_i} \left(P_{Load}(t) - P_{RES}(t)\right) \Delta t \\ & , \ldots , \sum_{t=t_{start\ shortage}}^{t_{equilibrium}} \left(P_{Load}(t) - P_{RES}(t)\right) \Delta t \geq 0 \Bigg] \end{aligned} \tag{5}$$

During the year under study, there may be several shortage periods. The shortage with the greatest amount of energy to store is selected. It is also possible that the system is always in deficit. In this case, the calculation of the amount of energy to be stored is stopped at the end of the year. The result provided by this pre-sizing assumes that the storage is perfect, i.e., that there are no losses due to the efficiency of the subsystems. This result is more of an indicator to characterize the chosen set of data than a sizing tool. To obtain a more realistic estimate of the amount of energy to be stored, the sign of $P_{Load}(t) - P_{RES}(t)$ for each sum needs to be checked. The function $f_{to\ or\ from\ stock}$ is used to take into account losses due to efficiency:

$$\begin{aligned} f_{to\ or\ from\ stock} : \left(P_{Load}(t) - P_{RES}(t)\right) \longmapsto & \\ if\ \left(P_{Load}(t) - P_{RES}(t)\right) < 0 : & \\ E_{stockage}(t) = \left(P_{Load}(t) - P_{RES}(t)\right) \times \eta_{to\ stock} & \\ else : & \\ E_{stockage}(t) = \left(P_{Load}(t) - P_{RES}(t)\right) / \eta_{from\ stock} & \end{aligned} \tag{6}$$

where $\eta_{to\ stock}$ is the efficiency of the subsystems that transform energy into its storable form, and $\eta_{from\ stock}$ is the efficiency of the subsystems that transform energy from its storable form into a form that can be used by consumers.

The following equation modifies the previous shortage indicator to take into account the efficiency of the storage chain:

$$\begin{aligned} E_{shortage,\eta} = Maximum \Bigg[& f_{to\ or\ from\ stock}\left(P_{Load}(t_{start\ shortage}) - P_{RES}(t_{start\ shortage})\right) \Delta t \\ & , \ldots , \sum_{t=t_{start\ shortage}}^{t_i} f_{to\ or\ from\ stock}\left(P_{Load}(t) - P_{RES}(t)\right) \Delta t \\ & , \ldots , \sum_{t=t_{start\ shortage}}^{t_{equilibrium}} f_{to\ or\ from\ stock}\left(P_{Load}(t) - P_{RES}(t)\right) \Delta t \geq 0 \Bigg] \end{aligned} \tag{7}$$

Assuming that during the shortage the H2 chain is the only source of storage, and assuming that energy management is perfect, i.e., it does not cause any losses or wastage of energy, an initial estimate of the quantity of hydrogen to be stored can be obtained by using hydrogen's lower heating value.

Table 2
Shortage indicator value in MWh for the worst (W) and best (B) combination of energy consumption and production data (year of load data/year of weather data) as a function of k_{power} and $k_{mix,pv}$.

k_{power}	$k_{mix,pv}$					
	0%		20%		40%	
	W	B	W	B	W	B
1	556 2020/2018	485 2022/2020	469 2020/2018	411 2020/2020	512 2022/2023	474 2020/2020
1,5	216 2019/2018	144 2022/2021	116 2020/2018	51 2020/2020	126 2020/2018	56 2020/2020
2	42 2020/2018	19 2022/2019	41 2020/2018	9 2022/2020	49 2022/2022	8 2019/2020
2,5	34 2020/2018	11 2022/2019	33 2022/2018	6 2023/2019	36 2020/2018	5 2019/2020
3	31 2020/2018	9 2021/2019	28 2020/2018	5 2020/2020	30 2020/2018	4 2019/2020
3,5	29 2020/2018	8 2021/2019	26 2020/2018	5 2023/2019	26 2020/2018	4 2019/2020

k_{power}	$k_{mix,pv}$					
	60%		80%		100%	
	W	B	W	B	W	B
1	671 2022/2023	641 2020/2021	880 2022/2023	852 2020/2021	1099 2022/2023	1072 2020/2021
1,5	198 2022/2023	158 2020/2020	457 2022/2023	430 2020/2021	777 2022/2023	754 2023/2022
2	77 2022/2023	30 2020/2020	191 2022/2023	134 2023/2018	474 2022/2023	453 2023/2022
2,5	47 2022/2022	6 2023/2020	124 2022/2023	68 2020/2020	323 2022/2023	259 2020/2021
3	35 2022/2018	5 2023/2020	69 2022/2022	28 2023/2020	286 2022/2023	218 2019/2018
3,5	29 2022/2018	4 2019/2020	46 2022/2022	8 2023/2020	251 2022/2023	180 2019/2018

The shortage indicator enables the system to be pre-sized, giving an idea of the quantity of energy to be stored. Although it requires a more complex simulation to be realistic, this quantity of energy to be stored is an indicator of the size of the system to be installed, and therefore its cost. As this sizing approach is simplified, the calculation results are only sensitive to energy production data from renewable sources and consumption data. This is a way of distinguishing between the years in which the combination of energy consumption and production conditions is favorable, and those in which this combination is unfavorable, thus influencing the overall cost of energy.

Having chosen to scale energy production and consumption data to the equivalent of the average water and electricity consumption of 200 inhabitants per year, as prescribed by Eq. (4), the difference in results between a favorable and unfavorable combination of input data depends only on the hour-by-hour variability of production and consumption. All the shortage values for the different scenarios are shown in Table 2. These different scenarios will serve as input data for the numerical model, the details of which are developed in the following section.

3. Numerical model

The scenarios presented in the previous section enable a balance to be drawn between the energy produced by renewable sources and the energy consumed over a one-year period. The main objective of the numerical model is to calculate the cost of the energy produced by the system for the benefit of users, as shown in the diagram of Fig. 2. Consequently, the system's performance has been assessed, i.e., the proportion of energy that can be redistributed to consumers as a function of the energy produced by renewables. Assuming that system performance is not too sensitive to degradation, it can be assumed that the system will perform the same from one year to the next. This simplification makes it possible to evaluate the total energy distributed to users over the life of the project on the basis of one-year calculations, i.e., by multiplying the results obtained over one year by the number of years in the life of the project.

Table 3
Main technical and economic parameters and assumptions for renewable energy sources.

RES parameters	
Photovoltaic solar panel cost	500 € m^{-2}
Photovoltaic solar panel area per kWp installed	4.70 m^2 kWp^{-1}
Cost of a wind turbine	85000 €

The other step in obtaining the energy cost is to account for all costs incurred during the life of the project. This includes investment costs for each of the subsystems, maintenance costs, but also the cost of replacing components that have a limited lifespan. These include batteries, fuel cells and electrolyzers (see Tables 3–6). These replacements are due to their utilization rate, in other words, the amount of energy charged and discharged from these systems. These steps in the energy cost calculation justify the decomposition of the numerical model into several sub-models:

- a performance model to calculate the energy redistributed to users and the component utilization rate;
- an ageing model to estimate the number of component replacements over the life of the project;
- an economic model that accounts for all fixed and variable costs (see Tables 3–6).

3.1. Performance model

To account for the evolution of the system, the model needs to track four quantities, each of which corresponds to a storage level:

- electricity, SOC (state of charge);

Table 4
Main technical and economic parameters and assumptions for batteries.

BT	
Battery bank 1 discharging efficiency $\eta_{BT1,-}$	0.95
Battery bank 1 converter efficiency $\eta_{CONV,BT1}$	0.95
Battery bank 1 C-Rate $Cr_{BT,1}$	2.00
Battery bank 1 investment cost $C_{inv,\ BT1,\ €/\ kWh}$	550 € kWh^{-1}
Battery bank 1 replacement cost	550 € kWh^{-1}
Lifetime battery bank 1 L_{BT1}	10 years
Maximum state of charge of battery bank 2 SOC_{max}	1.00
Minimum state of charge of battery bank 2 SOC_{min}	0.50
Initial state of charge of battery bank 2 SOC_{ini}	0.50
Battery bank 2 charging efficiency $\eta_{BT2,+}$	0.85
Battery bank 2 discharging efficiency $\eta_{BT2,-}$	0.85
Battery bank 2 converter efficiency $\eta_{CONV,BT2}$	0.95
Battery bank 2 investment cost $C_{inv,\ BT2,\ €/\ kWh}$	250 € kWh^{-1}
Battery bank 2 replacement cost	250 € kWh^{-1}

- hydrogen, LOH (level of hydrogen);
- drinkable water, LOW1 (level of drinkable water);
- pure water, LOW2 (level of pure water).

One of the objectives of the performance model is to take stock of these quantities at each time step and to report on their evolution. The model seeks to describe the relationships between these different quantities. At each time step, the simulated EWMS performs an energy balance. The diagram of Fig. 1 describes C3POe system, using the average power P_X consumed or produced by each subsystem X seen by the EWMS at AC bus level and implied in the model equations. These average powers are converted into energy by multiplying by the simulation time step:

$$\underset{[Wh]}{E_X} = \underset{[W]}{P_X} \times \underset{[h]}{\Delta_t} \tag{8}$$

Based on the same principle, the flows Q_X in the water circuit consumed or produced by the reverse osmosis systems or the electrolyzer are calculated at each time step to determine the evolution of water levels. The quantities of energy or water exchanged between the various subsystems will depend on the efficiency of each and the transformations carried out. Converters are used to adapt the electrical current to the AC bus. To account for these conversions, their efficiency is included in power calculations, and denoted by $\eta_{CONV,X}$, where X is the abbreviation for the subsystem for which the current converter is used.

3.2. Subsystems performance

The power range of the electrolyzer is defined between a high $P_{EL,UB}$ and a low power $P_{EL,LB}$:

$$\frac{P_{EL,LB}}{\eta_{EL,ac/dc}} < P_{EL}(t) < \frac{P_{EL,UB}}{\eta_{EL,ac/dc}} \tag{9}$$

where $P_{EL,LB}$ is the electrolyzer's lower operating limit and $P_{EL,UB}$ its upper limit. It is assumed that the electrolyzer's production and consumption of pure water are proportional to the power consumed. The efficiency of the electrolyzer η_{EL} is therefore assumed to be constant. The electrolyzer's lower operating limit $P_{EL,LB}$ is set at 30% of its rated power, which corresponds to an operating regime where its efficiency is close to its optimum [9]. The upper limit $P_{EL,UB}$ is set at the electrolyzer's rated power. The choice of these parameters makes it possible to limit errors due to the approximation of a constant efficiency, as the real efficiency of most electrolyzers varies little in this power range. It is assumed that the use of batteries coupled with appropriate energy management rules will enable the electrolyzer to operate in this range of use, where its efficiency is at its best.

The number of kg of hydrogen produced $k_{EL,P->H2}[kg\ Wh^{-1}]$ and the quantity of pure water consumed $k_{EL,P->Q}[m^3\ Wh]$ per Wh consumed are used to calculate the mass of hydrogen $\dot{m}_{H2}[kg\ h^{-1}]$ and the quantity of water $Q_{EL}(t)[m^3\ h^{-1}]$ produced per unit of time.

$$\dot{m}_{H2,+}(t) = k_{EL,P->H2} P_{EL}(t) \eta_{CONV,EL} \tag{10}$$

$$Q_{EL}(t) = k_{EL,P->Q} P_{EL}(t) \eta_{CONV,EL} \tag{11}$$

The power range of the fuel cell is defined between a high $P_{FC,UB}$ and a low power $P_{FC,LB}$:

$$P_{FC,LB} * \eta_{FC,dc/ac} < P_{FC}(t) < P_{FC,UB} * \eta_{CONV,FC} \tag{12}$$

The amount of energy produced as a function of the number of kg of hydrogen consumed is calculated from the assumed constant average efficiency η_{FC} and the lower heating value of hydrogen $LHV_{H2} = 33330\ [Wh\ kg^{-1}]$:

$$P_{FC}(t) = \dot{m}_{H2,-}(t) LHV_{H2}\ \eta_{FC}\ \eta_{CONV,FC} \tag{13}$$

To ensure that the assumption of constant efficiency remains valid, the upper limit of the fuel cell's working power is set at 80% of its rated power, and its minimum working power is set at 10%. In this operating range, efficiency is better, varying by around 7 or 8% [9]. This can be explained by the fact that as the electrical power output decreases, so does the efficiency of the fuel cell, but at low powers the consumption of auxiliaries reduces the overall efficiency of the system. This assumption, chosen to limit model errors, may have an influence on the overall cost of the system. Operating the fuel cell at a power level 20% lower than its rated power means that the fuel cell has to be oversized. As the cost of the fuel cell is a function of its rated power, the overall cost of the system is increased.

At each time step, the quantity of hydrogen in the tank changes according to the quantity produced by the electrolyzer and consumed by the fuel cell is calculated from hydrogen tank capacity $C_{H2}[kg]$:

$$LOH(t+1) = LOH(t) + \frac{k_{EL,P->H2} P_{EL}(t) \eta_{EL,ac/dc} \Delta t}{C_{H2}} - \frac{P_{FC}(t) \Delta t}{C_{H2}\ PCI_{H2}\ \eta_{FC}\ \eta_{FC,dc/ac}} \tag{14}$$

$$LOH(t+1) - LOH(t) = \frac{\dot{m}_{H2,+}(t) - \dot{m}_{H2,-}(t)}{C_{H2}} \tag{15}$$

The two reverse osmosis units operate at their rated power and have been sized to meet the annual water needs of the population of the island of Molène. The pure water reverse osmosis unit (RO2) can only operate when the drinking water reverse osmosis unit (RO1) is in operation. They can be switched on or off and deliver a constant flow rate. The flow rate $Q_{RO1}(t)$ gives the production of drinking water intended for consumption. The flow rate $Q_{RO2}(t)$ gives the production of pure water. The drinking water produced by RO1 is distributed between the drinking water reservoir intended for consumption and the drinking water intended for the production of pure water. The RO2 system produces pure water but rejects drinking water. The drinking water flow rate can therefore take two values: $Q_{RO1,RO2-ON}$ when RO2 is running and $Q_{RO1,RO2-OFF}$ when RO2 is switched off. Assuming constant speed operation simplifies the rules of priority for water and energy management.

The cost of storing drinking water is not included in the overall cost, as the installations are assumed to already exist. However the drinking water storage capacity C_{W1} is used to determine when to switch RO1 on or off, and must therefore be taken into account in the model. The capacity of the pure water tank C_{W2} has also been fixed, the size of the tank has a negligible influence on the result of the economic calculations; however, it must be taken into account in the model as the level of the pure water tank determines whether the electrolyzer can be switched on or off. The drinking water level $LOW1$ (see Eq. (16)) and the pure water level $LOW2$ (see Eq. (17)) are calculated at each time step.

$$LOW1(t+1) = LOW1(t) + \frac{Q_{RO1}(t) \Delta_t}{C_{W1}} - \frac{Q_{Load}(t) \Delta_t}{C_{W1}} \tag{16}$$

Table 5
Main technical and economic parameters and assumptions for the hydrogen chain.

H2	
Maximum hydrogen tank level LOH_{max}	1.00
Minimum hydrogen tank level LOH_{min}	0.01
Lower heating value hydrogen LHV_{H2}	33330 Wh kg^{-1}
Hydrogen tank investment cost per kg stored $C_{inv,\ H2,\ €/\ kg}$	470 € kg^{-1}
Cost of annual hydrogen tank maintenance as a percentage of investment cost	2 € kg^{-1}
EL	
Upper boundary of electrolyzer power consumption as a percentage of rated power $P_{EL,UB}$	100%
Lower boundary of electrolyzer power consumption as a percentage of rated power $P_{EL,LB}$	30%
Efficiency of the electrolyzer and its auxiliaries η_{EL}	0.5
Quantity of hydrogen produced per Wh consumed $k_{EL,P->H2}$	0.0166 kg kWh^{-1}
Electrolyzer converter efficiency $\eta_{CONV,EL}$	0.95
Quantity of pure water consumed per kWh consumed $k_{EL,P->Q}$	0.00016 m^3 kWh^{-1}
Number of times electrolyzer switched on and off before failure $nb_{st,tot,EL}$	7500
Number of hours of electrolyzer operation before failure $nb_{h,tot,EL}$	80000
Investment cost of electrolyzer as a function of installed power rating $C_{inv,\ EL,\ €/\ W}$	4.60 € W^{-1}
Cost of annual electrolyzer maintenance as a percentage of investment cost	4%
Replacement cost of electrolyzer stacks as a percentage of investment cost	26.7%
FC	
Upper boundary of fuel cell power consumption as a percentage of rated power $P_{FC,UB}$	80%
Lower boundary of fuel cell power consumption as a percentage of rated power $P_{FC,LB}$	10%
Efficiency of the fuel cell and its auxiliaries η_{EL}	0.50
Fuel cell converter efficiency $\eta_{CONV,EL}$	0.95
Number of times fuel cell switched on and off before failure $nb_{st,tot,FC}$	10000
Number of hours of fuel cell operation before failure $nb_{h,tot,EL}$	30000
Investment cost of fuel cell as a function of installed rated power $C_{inv,\ FC,\ €/\ W}$	3.9 € W^{-1}
Cost of annual electrolyzer maintenance as a percentage of investment cost	4%
Replacement cost of fuel cell stacks as a percentage of investment cost	27%

Table 6
Main technical and economic parameters and assumptions for the reverse osmosis systems.

RO1	
Rated power of reverse osmosis system 1 $P_{RO1,rated}$	11.4 kW
Drinking water flow rate, reverse osmosis system 2 is off $Q_{RO1,RO2-OFF}$	1.90 m^3 h^{-1}
Drinking water flow rate, reverse osmosis system 2 is on $Q_{RO1,RO2-ON}$	1.25 m^3 h^{-1}
Drinking water tank capacity C_{W1}	300 m^3
End-of-priority drinking water tank level $LOW1_{end\ priority}$	0.80
Start-of-priority drinking water tank level $LOW1_{start\ priority}$	0.10
Reverse osmosis 1 system investment cost $C_{inv,RO1}$	202 k€
Cost of replacing a reverse osmosis system membrane $C_{rep,RO1,membrane}$	12 k€
Reverse osmosis 1 system operating time before membrane replacement $t_{rep,RO1,membrane}$	15000 h
Cost of replacing consumables $C_{rep,RO1,consumables}$	1.2 k€
Reverse osmosis 1 system operating time before membrane replacement $t_{rep,RO,consumables}$	1000 h
Reverse osmosis 1 system fixed replacement costs $C_{rep,RO1,fixed}$	3.5 k€
RO2	
Rated power of reverse osmosis system 2 $P_{RO2,rated}$	1.3 kW
Drinking water flow rate Q_{RO2}	0.65 m^3 h^{-1}
Pure water tank capacity C_{W2}	1 m^3
Maximum level of pure water tank $LOW2_{max}$	0.90
Minimum level of pure water tank $LOW2_{min}$	0.20
Investment cost of reverse osmosis system 2 $C_{inv,RO2}$	298 k€

$$LOW2(t+1) = LOW2(t) + \frac{Q_{RO2}(t)\Delta_t}{C_{W2}} - \frac{Q_{EL}(t)\Delta_t}{C_{W2}} \tag{17}$$

The BESS is divided into two benches. The first bench is responsible for balancing the grid, and is not considered as a storage source or a determining producer of the system. The state of charge (SOC) of this first bench is not calculated by the model itself. In order to dimension the capacity of the bench, it is necessary to be able to determine the minimum and maximum state of charge during its service life. The state-of-charge of this first bench cannot be calculated by the model, as to evaluate SOC variations a time step of the order of a second or millisecond should be adopted.

As a result, it is not possible to size the capacity of this battery bench using the optimization algorithm. However, it is possible to approximate it by estimating the maximum power $P_{max,grid}$ consumed on the grid:

$$C_{BT,1} = \frac{P_{max,grid}}{Cr_{BT1} * \eta_{CONV,BT1,-}} \tag{18}$$

where $C_{BT,1}$ is the capacity of this first battery bench and $Cr_{BT,1}$ is its C-rating. The second battery bench has the function of absorbing energy variations beyond one hour. The model calculates the average quantity charged or discharged from the battery between two time steps and ensures that the average state of charge remains between a minimum SOC_{min} and maximum value SOC_{max}. The average state of charge over the time step varies according to the following equation :

$$SOC(t+1) = SOC(t) + \frac{P_{BT2,+}(t)\cdot\Delta t\cdot\eta_{BT2,+}\cdot\eta_{CONV,BT2}}{C_{BT2}} - \frac{P_{BT2,-}(t)\cdot\Delta t}{\eta_{BT2,-}\cdot\eta_{CONV,BT2}\cdot C_{BT2}} \tag{19}$$

where $C_{BT,2}$ is the capacity of this battery bench, $P_{BT,d}$ is the average power of the battery in a discharge phase, and $P_{BT,c}$ is the average power of the battery in a charging phase.

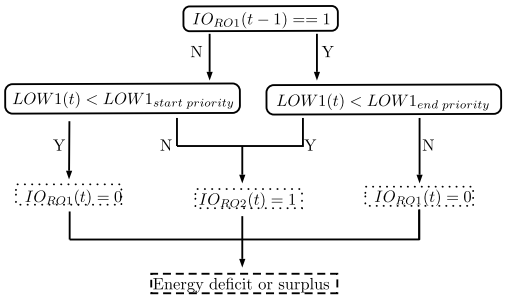

Fig. 8. Logic block diagram for switching the reverse osmosis (RO1) system producing drinking water on and off.

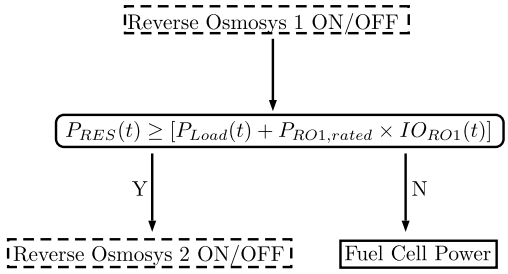

Fig. 9. Logical block diagram to define whether the system is in surplus or deficit.

3.3. Energy and water management system

The aim of the simulation is not to create a functional EWMS, but to integrate and simulate its behavior over the simulation time step, which is typically one hour (depending on the input data). As the simulation time step is one hour, the simulation cannot account for variations in power or flow rates over shorter time steps. So the simulated EWMS can only account for the major trends that will modify the state of the system. At each time step, the EWMS determines the electrical power consumed or produced on the AC bus by the various subsystems, based on the data provided by the scenarios, i.e., P_{RES}, P_{Load}, and Q_{Load}, as well as the value of the various levels, i.e., SOC, LOH, $LOW1$, and $LOW2$. In order to absorb grid fluctuations, priority is generally given to battery storage, followed by hydrogen storage. The battery state-of-charge and the level of the hydrogen tank are generally the key variables used to regulate the system.

The operating rules described above for each subsystem are taken into account in the operation of the simulated EWMS: On/off operations of the reverse osmosis systems, and control of the electrolyzer and fuel cell between high and low operating power. The EWMS operating rules are shown in the diagrams in Figs. 8 to 12. Energy management rules presented in Figs. 11 and 12 have been established from the ones described by Marocco et al. [4]. As shown in Fig. 8, the variation in the drinking water level is simulated at each time step by Eq. (16). Drinking water production becomes a priority when:

$$LOW1(t) < LOW1_{start\ priority} \longmapsto IO_{RO1}(t) = 1 \tag{20}$$

The priority stops when:

$$LOW1(t) > LOW1_{end\ priority} \longmapsto IO_{RO1}(t) = 0 \tag{21}$$

where IO_{RO1} is a variable indicating whether RO1 is running or stopped, $LOW1_{start\ priority}$ and $LOW1_{end\ priority}$ are two drinking water level values for which drinking water production becomes a priority or not. When $IO_{RO1}(t) = 1$, water requirements take priority, the reverse osmosis system will operate regardless of the state of the system (energy surplus or deficit). This configuration of the system makes it possible to respond to a water shortage. When $IO_{RO1}(t) = 0$, the reverse osmosis system unit operates only when there is an energy surplus and within the limits of the authorized drinking water level. The system must be capable of meeting the electrical needs of P_{Load} consumers at all times, i.e., the consumption of the electrical network cannot be controlled and cannot be shed. As shown in Fig. 9, after defining the water priority the simulated EWMS performs an initial energy balance by determining whether there is an energy surplus or deficit in relation to the electricity and water requirements:

$$P_{RES}(t) \geq \left[P_{Load}(t) + P_{RO1,rated} \times IO_{RO1}(t)\right] \tag{22}$$

As shown in Fig. 10 in the event of a surplus, energy is first stored in the battery bank. To ensure that the battery's SOC does not exceed its maximum limit SOC_{max}, the variable $P_{BT,SOC,+}$ is calculated at each time step:

$$P_{BT,SOC,+}(t) = \frac{C_{BT}\left[SOC_{max} - SOC(t)\right]}{\Delta_t \eta_{BT,+}} \tag{23}$$

The pure water level is then checked to see if there is enough to produce hydrogen. To ensure that the level of the pure water tank $LOW2$ does not exceed its minimum $LOW2_{min}$ or maximum limit $LOW2_{max}$, variables $Q_{LOW2,min}$ and $Q_{LOW2,max}$ are calculated at each time step, as shown respectively in Eq. (24) and (25). The RO2 system is switched on or off depending on the pure water level.

$$Q_{LOW2,min}(t) = \frac{C_{LOW2}\left[LOW2(t) - LOW2_{min}\right]}{\Delta_t} \tag{24}$$

$$Q_{LOW2,max}(t) = \frac{C_{LOW2}\left[LOW2_{max} - LOW2(t)\right]}{\Delta_t} \tag{25}$$

The remaining energy is used to determine the operating power of the electrolyzer, As shown in Fig. 11. To ensure that the level of hydrogen does not exceed its maximum limit LOH_{max}, the variable $P_{EL,LOH}$ is calculated at each time step:

$$P_{EL,LOH}(t) = \frac{C_{H2}(LOH_{max} - LOH(t))}{k_{EL,P->H2}\eta_{EL,ac/dc}\Delta t} \tag{26}$$

The variable P_{CURT} can be understood as the amount of energy not consumed by the system and users, or as the energy lost due to the curtailment of renewable energy production. In order of priority, energy from renewable sources is consumed by:

- water and electricity needs $\left(P_{Load} + IO_{RO1} \times P_{RO1,rated}\right)$;
- the recharging of the batteries $P_{BT,+}$, as long as the SOC remains between its upper and lower limits;
- the production of pure water P_{RO2};
- the production of hydrogen P_{EL};
- the loss of surplus energy P_{CURT}.

If the inequality Eq. (22) is not satisfied, the system is in energy deficit. As shown in Fig. 12 in the event of a deficit, energy is first taken from the BESS. To ensure that the battery's SOC does not fall below its minimum limit SOC_{min}, the variable $P_{BT,SOC,-}$ is calculated at each time step.

$$P_{BT,SOC,-}(t) = \frac{C_{BT}\left[SOC(t) - SOC_{min}\right]}{\Delta_t \eta_{BT,-}} \tag{27}$$

The fuel cell produces energy only when $LOH(t) > LOH_{min}$ and only in the permitted power range. As calculated in Eq. (28), the variable $P_{FC,LOH}(t)$ is used to determine the electrical power seen at the AC bus level produced by the fuel cell if it were to consume the quantity of H2 expressed in kg allowing the H2 tank to be emptied of its lower limit (LOH_{min}), i.e., $P_{FC}(t)$ must not exceed this power in order not to empty the $H2$ tank:

$$P_{FC,LOH}(t) = \frac{C_{H2}(LOH(t) - LOH_{min})\ PCI_{H2}\ \eta_{FC}\ \eta_{FC,dc/ac}}{\Delta t} \tag{28}$$

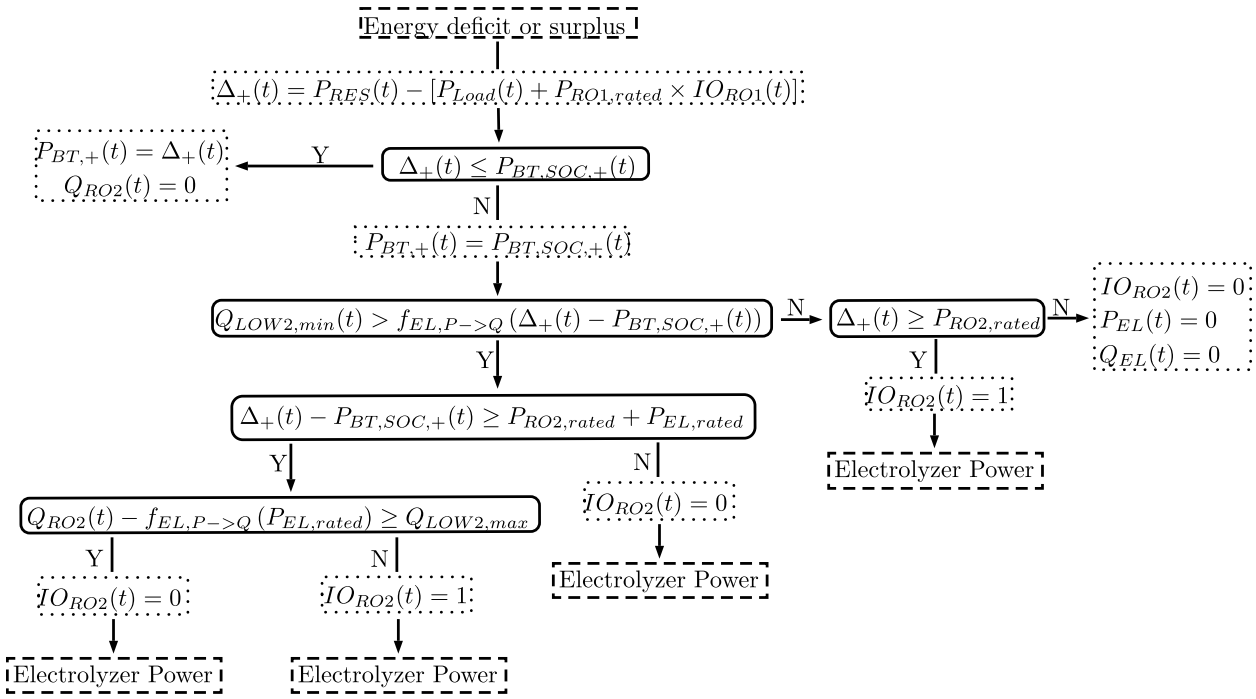

Fig. 10. Logic block diagram for switching the reverse osmosis (RO2) system producing pure water on and off.

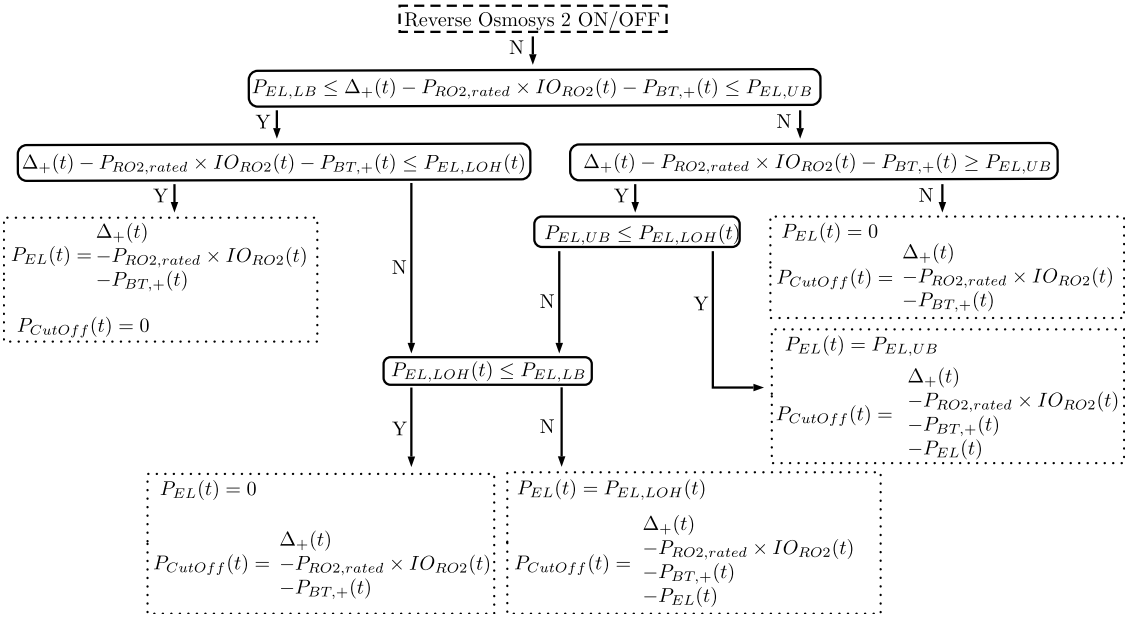

Fig. 11. Logic block diagram to define the electrolyzer's operating power.

Strictly speaking, the genset is not modeled, but a power P_{EXT} corresponding to an output of the model is calculated. This output variable is used to calculate the proportion of electricity consumed that comes from renewables. With the exception of the reverse osmosis unit 1, the other energy-consuming subsystems are shut down when the system has an energy deficit. In order of priority, the production of electricity to meet water and electricity requirements comes:

- from the renewable energy sources;
- from the battery bank, $P_{BT,-}$ as long as the SOC remains between its upper and lower limits;
- of the fuel cell, P_{FC};
- from a source external to the system P_{EXT}.

3.4. Ageing model

To define the overall performance of a system over a lifetime of several years, the first parameter often cited is system efficiency. However, the degradation quantifying the way in which the efficiency of subsystems degrades over time is often not yet fully taken into account in studies. Degradation is important because it makes it possible to assess how often the subsystems in use need to be replaced, generating

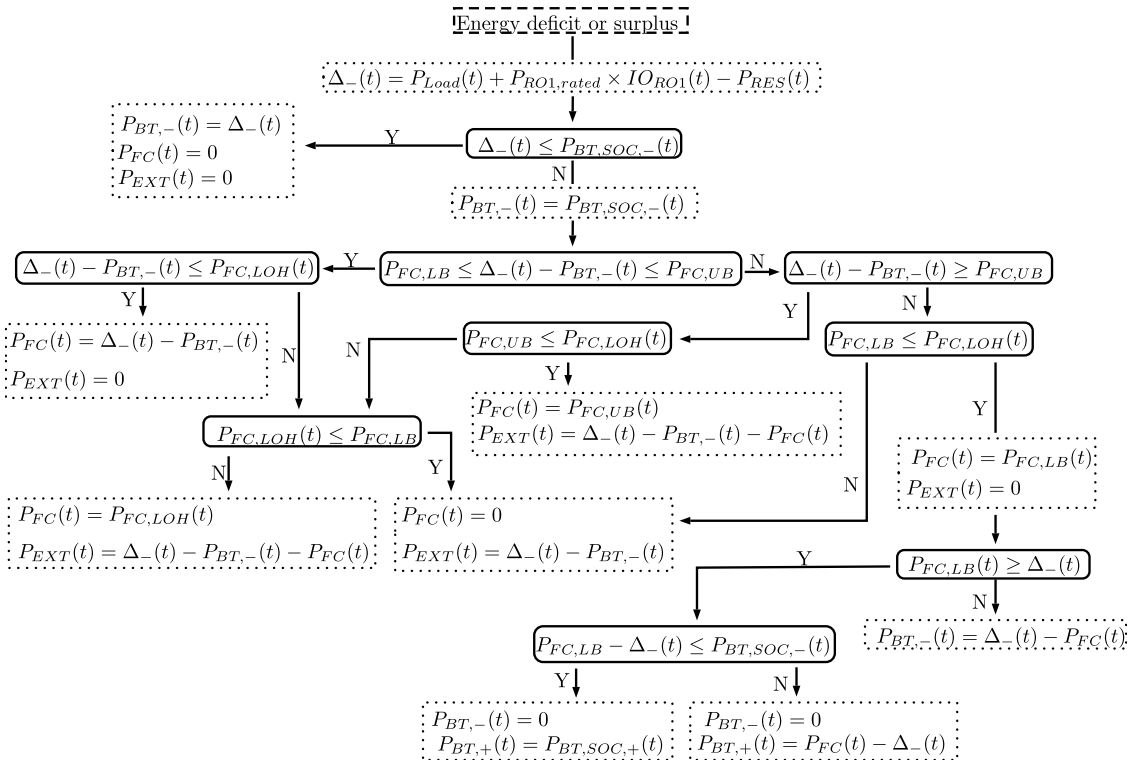

Fig. 12. Logic block diagram to define the Fuel Cell's operating power.

new investment costs and increasing the overall price of the system. In order to take into account the costs of maintaining and replacing the various components of the system over the life of the project (L_{PR}), it is necessary to use a set of models to estimate their aging and determine when they have to be replaced.

Both the fuel cell and the electrolyzer will run for many hours, and over time their performance will decline. As the fuel cell and electrolyzer operate within a long-term storage chain, both systems may experience cyclic load changes, start–stop succession, idling or high-power operation, which can accelerate their degradation. However, at the design stage, the future operating states of these systems are unknown, which means that the factors accelerating their degradation are unknown. In other words, future operating performances can only be estimated.

Li et al. have taken into account the performance degradation of an electrolyzer and a fuel cell within a microgrid using a model based on cell voltage [42]. The degradation of the electrolyzer will cause the cell voltage to increase and the degradation of the fuel cell will cause the cell voltage to decrease. In fact, this degradation model is based on the time they are in use. Le et al. estimate the hourly voltage degradation of cells in an electrolyzer and a PEM fuel cell at $+10\mu V/h$ and $-5\mu V/h$ respectively [43]. Based on a series of CFD simulations of a system based on photovoltaic solar panels and hydrogen storage, Ozden et al. estimate a two-year degradation in PEM fuel cell performance of 17% [22,44].

Pei et al. studied fuel cell performance degradation under different operating conditions in vehicle applications [45]. In on-board applications, the main feature is that fuel cells always operate at varying load conditions. The authors attribute over 50% of the performance degradations to these load changes, while frequent switching on and off accounts for around a third of the causes of degradation. El-kharouf et al. reviewed the main degradation mechanisms of PEM fuel cells to understand both the changes in membrane performance with time in various applications and the main phenomena causing degradation [46]. Yu et al. specifically studied the degradation of PEMFCs during shutdown and start-up processes [47]. Hua et al. carried out a review of PEMFC degradation mechanisms and, above all, of the models used to predict degradation [48]. However, the models studied, based on short and medium term performance trends, do not enable users to plan long-term maintenance operations. Jupiter 1000 is a Power-to-Gas industrial demonstrator in which an alkaline electrolyzer and PEM are tested. After 5 years of operation, the efficiency and causes of degradation of the electrolyzers have been reported [49].

PEM electrolyzers degrade more rapidly than alkaline electrolyzers. They can present an efficiency loss of 2.5% per year and have an estimated lifespans 2 to 5 times shorter than alkaline electrolyzers. Alkaline electrolyzers have a service life of around 90000 h and can show an efficiency loss of almost 1% per year [50,51]. Performance degradation is used to determine when the electrolysis stack or fuel cell should be replaced, usually when the energy efficiency drops to 90% of its initial nominal value [9]. Some models estimate replacement based on service life and operating time in hours [30,52]. But counting degradations in terms of hours presupposes that degradations are linear, which is debatable. Studying a system producing hydrogen from wind energy and a PEM electrolyzer, Santos et al. estimated efficiency degradation at 2% of rated power for 8,000 h of operation [53]. The authors report 5000 on/off switching cycles and an overall service life of 40000 h. Brauns and Turek, in their review of alkaline electrolyzers powered by renewable energies, report that these can tolerate between 5,000 and 10,000 on–off cycles [54].

Torreglessa et al. have developed an EMS for a HRES that takes the minimizing of the operating cost into account when deciding when to operate system components [55]. The authors report that one start of PEM FC from 0 to the rated power represents 3 working hours in continuous operation. They conclude performance degradation of the subsystems plays a key role in their analysis, but the results are subjected to the accuracy of the lifetime degradation models. The performance degradation of fuel cells and electrolyzers is widely studied in the literature, but the models accounting for their degradation remain uncertain. However, performance degradation and the cost of

Table 7
Values DOD-CTF BT2.

DOD %	CTF
10	5700
25	2100
35	1470
50	1000
60	830
70	700
80	600
90	450

replacement cannot be neglected. A calculation based on operating time and number of on–off cycles has already been used, and seems a good alternative in view of the modeling uncertainties involved [9]. We use here the same methodology used by Marocco et al. to determine the ageing and replacement of the fuel cell, electrolyzer and battery pack 2, and does not take into account the performance degradation of each of these subsystems. One of the practical reasons for this choice is that, in order to take into account annual performance degradations, the system's performance needs to be calculated over its total lifetime, which can potentially multiply the calculation time by L_{PR}.

The lifetime of the electrolyzer L_{EL} and fuel cell L_{FC} are calculated from their annual operating hours $nb_{h,XX}$ and the number of times they are switched on and off $nb_{st,XX}$ in the course of a year.

$$L_{EL} = min\left(\left(\frac{nb_{h,\,EL}}{nb_{h,\,tot,\,EL}} + \frac{nb_{st,\,EL}}{nb_{st,\,tot,\,EL}}\right)^{-1}, L_{PR}\right) \tag{29}$$

$$L_{FC} = min\left(\left(\frac{nb_{h,\,FC}}{nb_{h,\,tot,\,FC}} + \frac{nb_{st,\,FC}}{nb_{st,\,tot,\,FC}}\right)^{-1}, L_{PR}\right) \tag{30}$$

where $nb_{st,\,tot,\,XX}$ and $nb_{h,\,tot,\,FC}$ represent respectively the number of total cycles and the number of operating hours that the subsystems can perform before being replaced.

The life of the hydrogen tank is assumed to be equal to the life of the project. Generally, once the number of complete filling cycles of the tank has been reached, a check is carried out and if the check does not reveal any malfunction, the same number of complete filling cycles are repeated.

Battery life can be estimated on the basis of the life curve provided by the manufacturer, which illustrates different values of depth of discharge (DOD) and the corresponding number of cycles to failure (CTF). The DOD is the maximum fraction or percentage of a battery's capacity (expressed in Ah) that is regularly removed from the charged battery. For each depth of discharge, an amount of energy that can flow through the battery can be calculated. Assuming that the battery will experience the different depths of discharge in equal proportion over its lifetime, it is possible to calculate an average amount of energy that can be charged and discharged from the battery lifetime throughput (LT), the calculation of which is detailed in Eq. (31). The Table 7 gives DOD and CTF values for battery bank 1 [56].

$$LT = \sum_{i=1}^{n} \frac{2C_{BT2}DOD_i\ CTF_i}{n} \tag{31}$$

The amount of energy charged and discharged from the battery over one year, i.e. annual throughput (AT), is calculated by the model using the following equation:

$$AT = \sum_{t=1}^{8760}\left(P_{BT2,+}(t)\eta_{BT2,+}\eta_{CONV,BT2} + \frac{P_{BT,-}(t)}{\eta_{BT,-}\eta_{CONV,BT2}}\right) \tag{32}$$

Battery life can be deduced from this :

$$L_{BT2} = min\left(\frac{LT}{AT}, L_{PR}\right) \tag{33}$$

In practice, the one-hour modeling time step makes it impossible to assess the amount of energy charged or discharged from the first battery bank so its lifetime has been fixed to L_{BT1}. The membrane in the reverse osmosis system is one of the main components to be replaced. Its replacement will depend on the length of use. To this must be added a set of consumables that also depend on operating time. The replacement of these components are included in the economic model.

3.5. Economic model

The costs included in the simulation depend on the installed power rating of the components and the amount of energy generated, or on their utilization rate. This leads us to distinguish between investment costs, fixed maintenance costs and replacement costs. In this study, the logistical costs of transporting or installing the system in the area of use are not taken into account, as they are too difficult to determine at this stage of the project. The cost of drinking water storage is not taken into account, as it is assumed to already exist. As shown in Fig. 1, all costs relating to the subsystems included in the C3POe system are taken into account. The costs of renewable energy sources are calculated for each scenario according to the kWp of photovoltaic solar panels and the number of 20 kW wind turbines installed.

Most of the investment costs are assumed to be proportional to installed capacity or rated power. This simplifies the sizing problem by making the economic calculations continuous. The investment cost of the converters $C_{inv,CONV}$ will depend on the installed power or capacity of the subsystem being served. As reverse osmosis systems are already dimensioned, their costs are given in absolute values.

$$\begin{aligned} C_{inv} = {} & C_{inv,\,EL,\,€/\,W}P_{EL,\,rated} + C_{inv,\,FC,\,€/\,W}P_{FC,\,rated} + C_{inv,\,H2,\,€/\,kg}C_{H2} \\ & + C_{BT1}C_{inv,\,BT1,\,€/\,kWh} + C_{BT2}C_{inv,\,BT2,\,€/\,kWh} \\ & + C_{inv,CONV} \\ & + C_{inv,RO1} + C_{inv,RO2} \end{aligned} \tag{34}$$

The maintenance cost of the electrolyzer and fuel cell are calculated on the basis of the assumptions made by [4]. It is assumed to represent 4 % of the initial investment cost per year, and is broken down into a fixed cost per year for $\frac{2}{3}$, and a variable cost depending on the duration of use for $\frac{1}{3}$:

$$C_{om,EL/FC} = \frac{4}{100}\left(\frac{2}{3}C_{inv,EL/FC}\frac{nb_{h,\,EL/FC}}{8760} + \frac{1}{3}C_{inv,EL/FC}\right)L_{PR} \tag{35}$$

Maintenance costs for the hydrogen tank are estimated at 2% of the investment cost per year. Battery maintenance costs are neglected.

The replacement cost of the FC and EL depends on the lifetime of the project and the estimated lifetime of the cell stacks in years. They have been calculated on the basis of the assumptions made by [9]. The replacement cost expressed as a percentage of the initial investment cost is estimated at 26.7% for both systems.

Reverse osmosis system component replacement costs are based on the number of hours of operation. $nb_{h,RO1}$. This number of hours is used to determine the number of membrane replacements and the quantity of consumables used. In addition to the cost of replacing components, which depends on the number of operating hours, there is a fixed replacement cost every two years. The following equation is used to determine the cost of all the replacements $C_{rep,RO1}$ of the reverse osmosis systems:

$$C_{rep,RO1} = L_{PR}\left[nb_{h,RO1}\left(\frac{C_{rep,RO1,membrane}}{t_{rep,RO1,membrane}} + \frac{C_{rep,RO1,consumables}}{t_{rep,RO1,consumables}}\right) + \frac{C_{rep,RO1,fixed}}{2}\right] \tag{36}$$

For the Reverse Osmosis 2 system, only the investment cost is taken into account, while replacement and maintenance costs are neglected.

The battery replacement cost $C_{rep,BT}$ are calculated from their calculated lifetime and assumed to represent 50% of their investment cost. As mentioned above, the aim of the system is to meet 100% of consumers' demand. When the system is unable to provide this, the

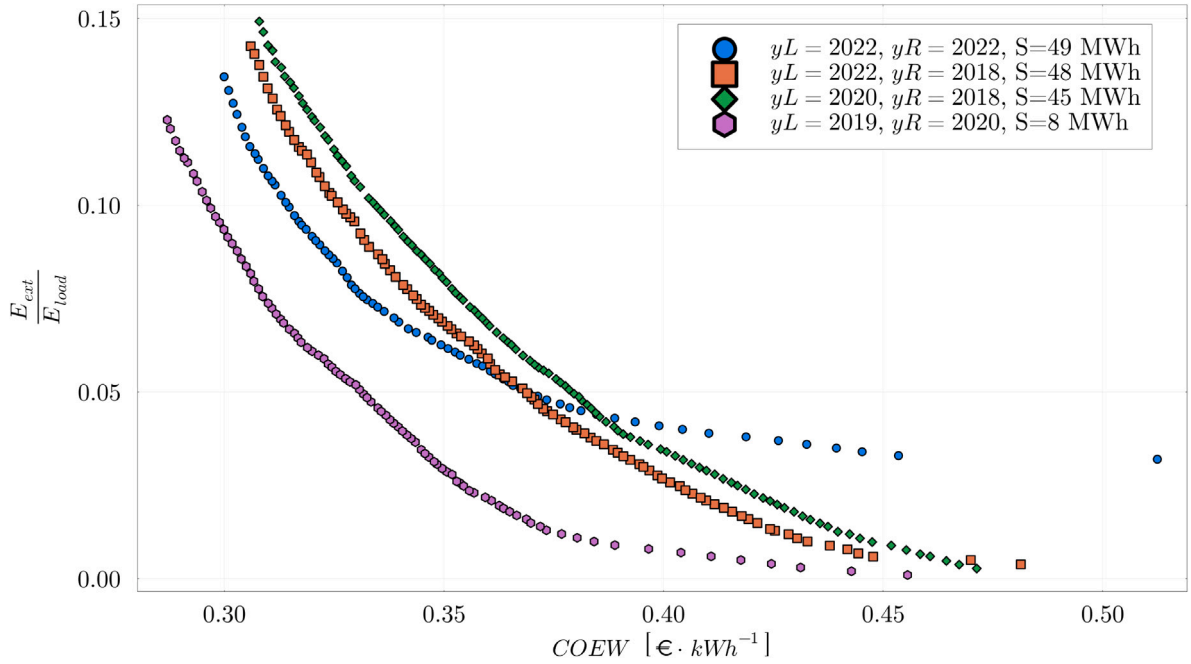

Fig. 13. Pareto fronts and shortage indicator calculated from multi-year data sets, for $k_{power} = 2$ and $k_{mix,pv} = 0.4$. With yL the year of consumption data, yR the year of meteorological data used to calculate energy production from renewables, and S the value of the shortage indicator.

assumption is made that the energy is supplied by a facility external to the system. The cost of this energy is based on the cost of producing energy on the Breton islands in 2022, i.e., 0.455 € kWh^{-1}:

$$C_{EXT} = 0.455 L_{PR} \sum_{t=1}^{8760} P_{EXT}(t) \tag{37}$$

For each scenario, the cost of renewable energies C_{RES} is calculated and depends on the installed capacity.

4. Sizing methodology

The model described above gives the cost of the system over its lifetime and the energy produced or consumed. Four parameters were used to size the system: the rated power of the electrolyzer and fuel cell, the capacity of battery bank 2 in kWh, and the capacity of the hydrogen tank in kg of H2. By varying these parameters, the cost of energy is modified. The overall sizing approach consists of varying these parameters to minimize the indicators or functions chosen as objectives. Colla et al. have reviewed the various indicators used to assess the competitiveness of energy projects [57]. The most commonly used indicator is the levelized cost of energy (LCOE). However, this indicator is criticized by some authors, who propose other indicators to replace it [57–61]. These authors argue that the LCOE distorts comparisons between different energy projects, and puts projects based on renewable resources at a disadvantage compared to those based on fossil fuels. It inaccurately disadvantages resource types whose costs are concentrated at the beginning of the period, with the distortion increasing with discount rates and the length of the analysis period.

From a sizing point of view, this indicator adds another parameter, the discount rate, which is estimated and assumed to be known in most studies, which can distort the results. For these reasons, the simpler indicator of the cost of energy and water has been opted as a first objective function.

$$COEW = \frac{C_{inv} + C_{om} + C_{rep} + C_{EXT} + C_{RES}}{L_{PR} \sum_{t=1}^{8760} P_{Load}(t)} \tag{38}$$

This indicator should not be interpreted as the actual cost that the consumer will have to pay for electricity and water over the life of the project, but as an optimization objective. First of all, the cost of energy and water are correlated. As discussed in this article, the actual cost will depend on weather conditions, users' consumption habits, which may change, future inflation and interest rates, among other things. Furthermore, this article does not pretend to take into account all the sensitive phenomena that can influence energy costs. The model does not take into account deterioration in annual performance, among other things. Furthermore, as previously discussed, electrolyzer and fuel cell efficiency are assumed to be fixed and not dependent on operating power. Before providing an estimate on a real cost, a sensitivity study has to be carried out on each of the parameters assumed to be known, to measure the influence of each of the sub-models used and the assumptions taken into account. This will be the subject of a future study.

The second objective taken into account is the share of energy from outside the system in the total energy consumed by users as shown in Fig. 7. Greenhouse gas emissions depend directly on the share of fossil fuels in the energy mix, and by minimizing this second objective, greenhouse gas emissions are diminished.

$$\frac{E_{EXT}}{E_{Load}} = \frac{\sum_{t=1}^{8760} P_{EXT}(t)}{\sum_{t=1}^{8760} P_{Load}(t)} \tag{39}$$

The aim of the C3POe project is to replace fossil fuel-based power generation systems. The two main decision-making criteria are the energy cost of the new system and the proportion of energy from renewable sources.

The Borg multi-objective evolutionary algorithm has been chosen for the minimization of the two objective function [62–66]. The Borg MOEA is not a single algorithm; instead it represents a class of algorithms whose operators are adaptively selected based on the problem. This algorithm was chosen for its flexibility, allowing the model to evolve in the future (add sub-models, objective functions, or other parameters for sizing). The Borg MOEA algorithm was configured with an epsilon value of $\epsilon = 0.001$ and a maximum number of 100,000 iterations. The calculations were carried out on a computing station equipped with a 36-core processor. The calculation time to optimize the model parameters for a scenario using a single core varies between 15 and 20 h. By parallelizing the calculations on the 36 cores, the

calculation time for the 36 scenarios is thus limited to 20 h, instead of one month if the calculations had been carried out on a single core. This substantial calculation time justifies the simplifications previously carried out on the model, and demonstrates the value of the shortage indicator in limiting the number of calculations by selecting the most relevant input data to best size a system. The results presented in the next section validate the use of the shortage indicator by performing optimizations with data sets from different years.

5. Results and discussion

5.1. Pareto front analysis

In the first instance, it is important to understand the limitations of the selection of the input dataset based on the shortage indicator. The graph in Fig. 13, shows the Pareto fronts and shortage indicator calculated from multi-year data sets, for $k_{power} = 2$ and $k_{mix,pv} = 0.4$. Each Pareto front is calculated from a pair of data sets (yL, yR), where yL is the year of consumption data, and yR is the year of meteorological data used to calculate energy production from renewables. It is difficult to determine qualitatively which is the best Pareto front when the shortage indicator values are close, i.e. for pairs (2022,2022), (2022,2018), (2020,2018), and for pairs (2023,2020), (2020,2020), (2019,2020). It might be advisable to choose data sets for which the shortage indicator value is close, to make the results more reliable. However, to limit the number of calculations, only those pairs of datasets for which the shortage indicator is the best and the worst have been retained. The aim is to estimate the margin of error in calculating Pareto fronts when pairs of data sets are chosen randomly or chronologically, or when data from a single year of production or consumption is used.

The optimization algorithm is used for each of the scenarios presented in Table 2. As shown in Fig. 14 for each scenario, there is a clear difference between the results obtained from a favorable and unfavorable data set. This confirms that the shortage indicator is sufficiently sensitive to characterize the input data sets. Each point on the Pareto fronts corresponds to a system configuration optimized to minimize COEW and $\frac{E_{EXT}}{E_{Load}}$. The Pareto fronts shown in Fig. 14 are obtained from energy mixes composed of 40% photovoltaics and 60% of wind power. This comparison between the different Pareto fronts makes it possible to establish the best k_{power} factor for a fixed $k_{mix,pv}$ factor. In Fig. 14, the best Pareto fronts are obtained for $k_{power} = 2.0$. However, increasing the installed renewable power capacity by taking $k_{power} = 2.5$ makes it easier to reach the 100% renewable energy target, at the expense of a slightly higher energy cost. As shown in Fig. 15, with a 100% photovoltaic energy mix, the cost of energy is much higher. Also, it is impossible to reach the 100% renewable energy target even if the amount of renewable energy injected is drastically increased. This result can be explained by comparing the profiles of photovoltaic energy production, see Fig. 3 and energy consumption, see Fig. 6. Photovoltaic energy production is low in winter but high in summer, while energy consumption is high in winter and lower in summer. The set of best Pareto fronts obtainable for each value of $k_{mix,pv}$ is shown in Fig. 16. It should be noted here that while the shortage indicator can be used to distinguish between data with the best and worst conditions, it cannot be used to rank the results of different scenarios, i.e. for different renewable energy production mixes. If the energy mix remains unchanged, the cost of renewable energies varies little between two sets of data, but the cost of system components may be optimized, to best adapt to the gap between consumption and production of renewable energies measured by the shortage indicator. This Pareto front analysis is a first step towards finding a suitable system sizing. Energy cost and $\frac{E_{EXT}}{E_{Load}}$ are two decision criteria that will vary according to consumption and weather conditions over the life of the project. A study based on sets of favorable and unfavorable results provides an estimate of the range of variation in energy cost over the life of the system. As already mentioned, the choice of a renewable energy mix is a complex one. A study of Pareto fronts provides an additional decision criterion for establishing the consequences of this choice on the cost of energy and the proportion of renewables.

5.2. Study of a specific scenario

For the purposes of this article, and in order to better explain the sizing approach presented here, the scenario with $k_{mix,pv} = 0.4$ and $k_{power} = 2.0$ is selected. Optimization was used to determine the model parameters minimizing COEW and the $\frac{E_{EXT}}{E_{Load}}$ ratio. The input data pair selected for these optimizations corresponds to the years (2022/2022) for unfavorable conditions and (2019/2020) for favorable conditions. As shown in Fig. 13, the Pareto front obtained with the (2020/2018) dataset intersects with that obtained with the (2022/2022) dataset. The aim of this scenario study is to determine a high and low margin for the COEW and the $\frac{E_{EXT}}{E_{Load}}$ ratio. Consequently, the Pareto front obtained with the data set (2020/2018) is also studied. Using the parameters obtained from the optimization of these three Pareto fronts, COEW and $\frac{E_{EXT}}{E_{Load}}$ have been calculated from the 36 combinations of consumption and meteorological data sets from 2018 to 2023. The minimum and maximum values for COEW and the $\frac{E_{EXT}}{E_{Load}}$ ratio are then used, as shown in Fig. 17, Fig. 18, and Fig. 19 corresponding respectively to the Pareto fronts obtained from the data sets for years (2019/2020), (2022/2022), and (2020/2018). By combining the 3 Pareto fronts, a framework for the two optimization objectives is obtained.

For the sake of brevity, only those points on the Pareto front for which $COEW \approx 0.35€\ \mathrm{kWh}^{-1}$ have been selected. Table 8 shows the calculation points extracted from the Pareto front obtained from good consumption and weather conditions, (2019/2020) dataset. Table 9 shows the calculation points extracted from the Pareto front obtained from bad consumption and weather conditions, i.e. (2022/2022) dataset. Table 10 shows the calculation points extracted from the Pareto front obtained from the (2020/2018) dataset.

This sequence of calculations illustrates that sizing based on fixed input conditions does not guarantee an energy cost, but gives an approximation of it. This is essential for validating parameters, but also for testing system flexibility. In the overall dimensioning approach, the minimum and maximum values of COEW and $\frac{E_{EXT}}{E_{Load}}$ has to be considered to determine the choice of a parameter set.

6. Study of a specific system configuration

For the sake of brevity, only the parameter set shown in the first line of Table 9 have been retained to present the following results in the remainder of this article. The graph in Fig. 21 shows, hour by hour, the energy delivered to the consumer and its origin. A large proportion of this energy $P_{RES \mapsto Load}$ comes directly from renewables without passing through the C3POe system, as shown in Table 11. Although representing only 6.28% of the total, external energy sources P_{EXT} have the highest power demand. This is mainly in winter, when the system experiences the greatest energy deficit, as shown in the graph in Fig. 20. As the graph in Fig. 23 shows, during this period the hydrogen tank is empty. In a real-life situation, this demand for power is problematic, and would probably cause a network blackout. As part of a system sizing approach, the maximum value of P_{EXT} could be taken into account as a 3rd optimization objective.

To reduce this demand for power, various energy management strategies can be envisaged, while minimizing energy costs. This discussion is beyond the scope of this article, but illustrates the dependence of the sizing strategy on energy management. The graph in Fig. 22 shows the energy consumed hour by hour by the electrolyzer, the reverse osmosis systems, or charged to the battery, as well as the energy from renewables lost by the system. The Table 12 gives the distribution of energy consumption from renewable sources. Around a third of energy from renewables is lost. Strictly speaking, it is not possible to

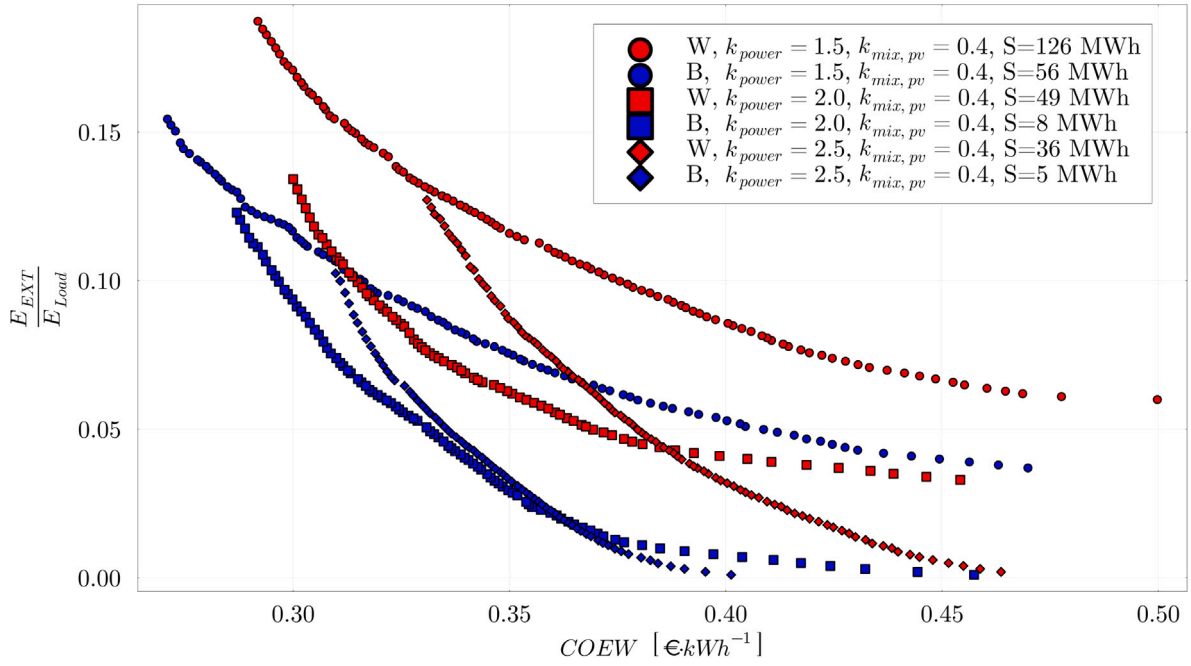

Fig. 14. Pareto front for scenarios with 60% wind renewable energy and 40% photovoltaic renewable energy and different values of k_{power}. The red Pareto fronts show the results obtained with input data for which the shortage indicator S is maximal. Pareto fronts in blue represent results obtained with input data for which the shortage indicator S is minimal.

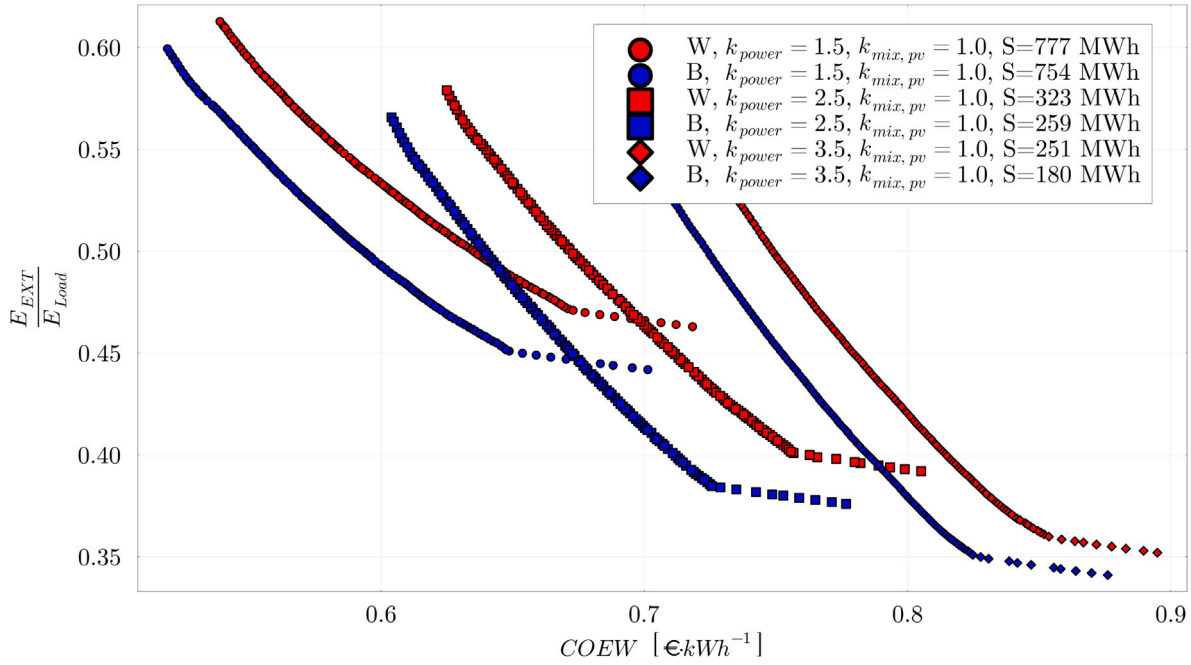

Fig. 15. Pareto front for scenarios with 100% photovoltaic renewable energy and different values of k_{power}. The red Pareto fronts show the results obtained with input data for which the shortage indicator S is maximal. Pareto fronts in blue represent results obtained with input data for which the shortage indicator S is minimal.

Table 8
Optimized system parameters obtained from the (2019/2020) dataset for a $COEW \approx 0.35$ € kWh^{-1}, $P_{EL,rated}$ rated power of the electrolyzer in [W], $P_{FC,rated}$ rated power of the fuel cell in [W], C_{BT} capacity of the battery bank 2 in [Wh], and C_{H2} the capacity of the hydrogen tank in [kg] of H2.

COEW	$\frac{E_{EXT}}{E_{Load}}$	$COEW_{max}$	$COEW_{min}$	$\left(\frac{E_{EXT}}{E_{Load}}\right)_{max}$	$\left(\frac{E_{EXT}}{E_{Load}}\right)_{min}$	C_{BT} [Wh]	C_{H2} [kg]	$P_{EL,rated}$ [W]	$P_{FC,rated}$ [W]
0.350	0.029	0.371	0.350	0.061	0.029	23014	368	46887	54781
0.351	0.029	0.372	0.351	0.060	0.029	28073	373	47552	53844

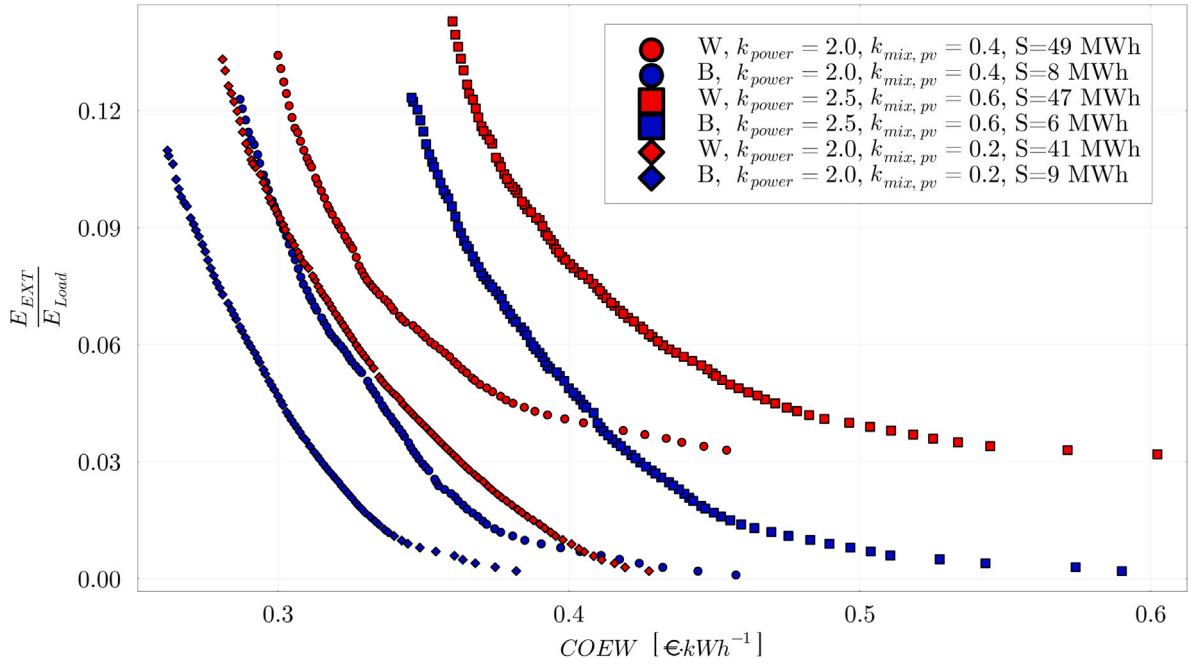

Fig. 16. Pareto front for best selected k_{power} for each $k_{mix,pv}$. The red Pareto fronts show the results obtained with input data for which the shortage indicator S is maximal. Pareto fronts in blue represent results obtained with input data for which the shortage indicator S is minimal.

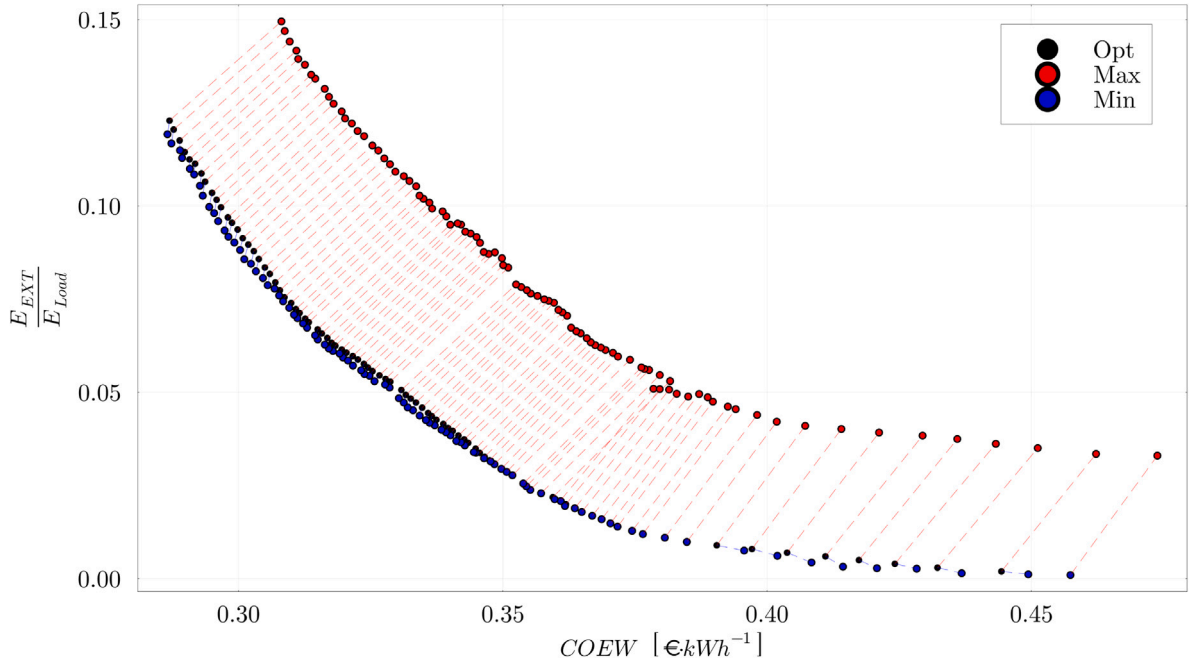

Fig. 17. Maximum (MAX) and minimum (MIN) value of COEW and $\frac{E_{EXT}}{E_{Load}}$ ratio calculated and determined for each point (i.e. optimized system configuration) of the Pareto front (2019/2020) based on 36 combinations of consumption and weather data from 2018 to 2023.

Table 9
Optimized system parameters obtained from the (2022/2022) dataset for a $COEW \approx 0.35$ € kWh^{-1}, $P_{EL,rated}$ rated power of the electrolyzer in [W], $P_{FC,rated}$ rated power of the fuel cell in [W], C_{BT} capacity of the battery bank 2 in [Wh], and C_{H2} the capacity of the hydrogen tank in [kg] of H2.

COEW	$\frac{E_{EXT}}{E_{Load}}$	$COEW_{max}$	$COEW_{min}$	$\left(\frac{E_{EXT}}{E_{Load}}\right)_{max}$	$\left(\frac{E_{EXT}}{E_{Load}}\right)_{min}$	C_{BT} [Wh]	C_{H2} [kg]	$P_{EL,rated}$ [W]	$P_{FC,rated}$ [W]
0.349	0.063	0.358	0.336	0.072	0.043	6577	208	43466	52003
0.351	0.062	0.359	0.337	0.072	0.042	6636	230	43466	52003

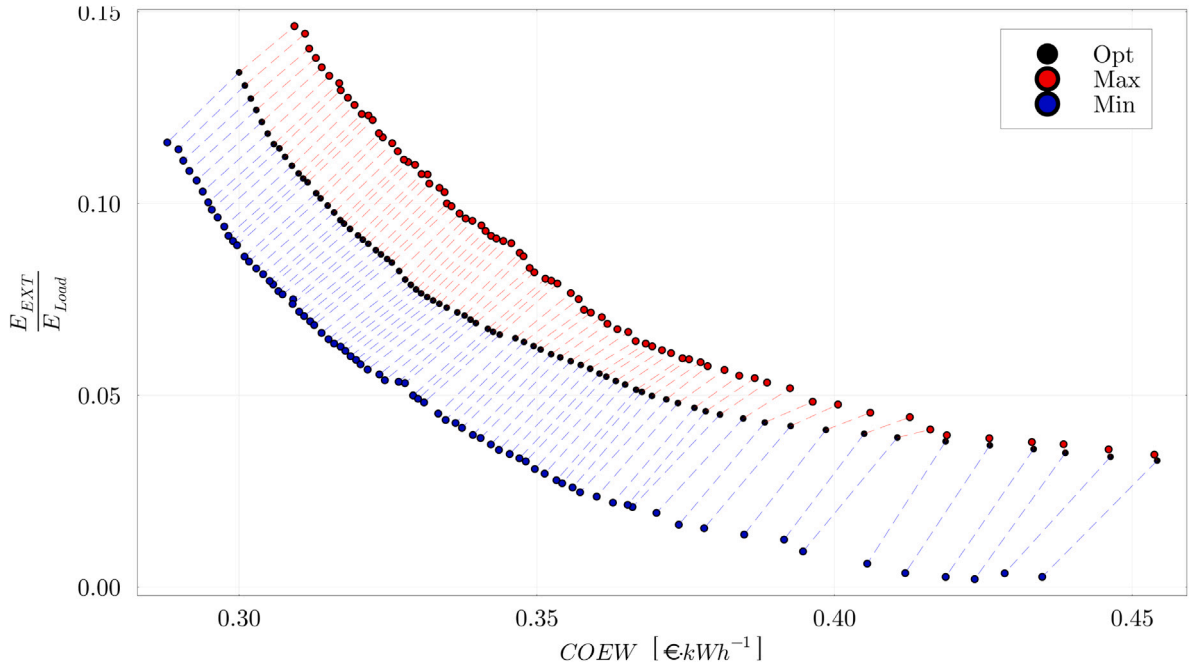

Fig. 18. Maximum (MAX) and minimum (MIN) value of COEW and $\frac{E_{EXT}}{E_{Load}}$ ratio calculated and determined for each point (i.e. optimized system configuration) of the Pareto front (2022/2022) based on 36 combinations of consumption and weather data from 2018 to 2023.

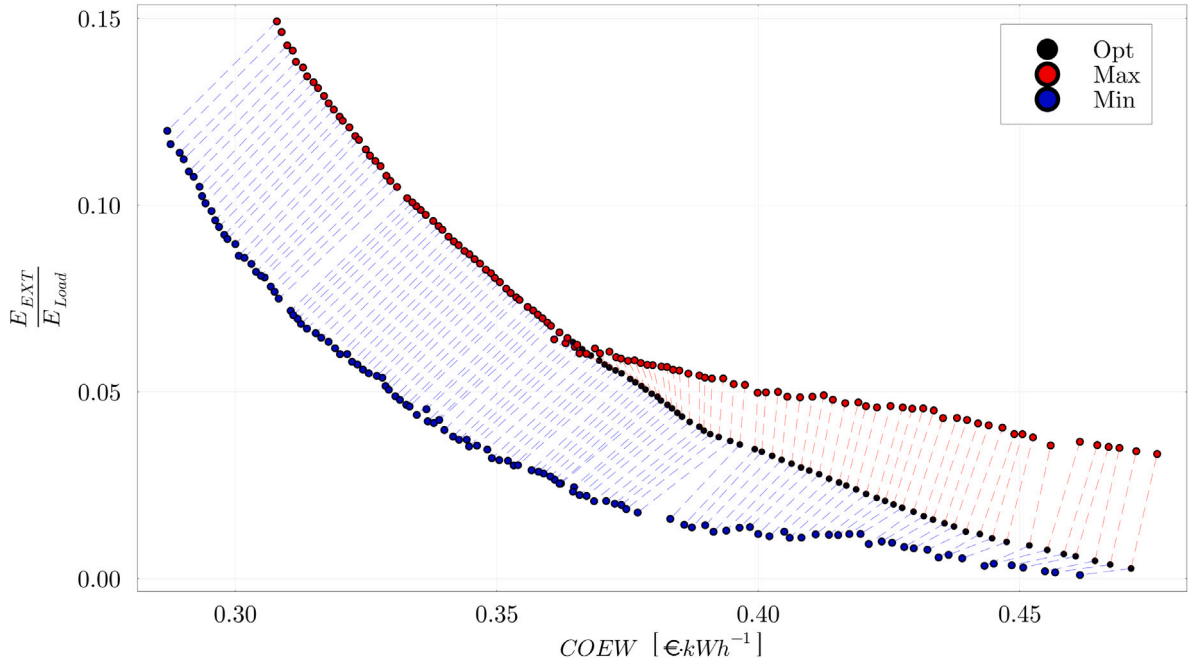

Fig. 19. Maximum (MAX) and minimum (MIN) value of COEW and $\frac{E_{EXT}}{E_{Load}}$ ratio calculated and determined for each point (i.e. optimized system configuration) of the Pareto front (2020/2018) based on 36 combinations of consumption and weather data from 2018 to 2023.

Table 10
Optimized system parameters obtained from the (2020/2018) dataset for a $COEW \approx 0.35$ € kWh^{-1}, $P_{EL,rated}$ rated power of the electrolyzer in [W], $P_{FC,rated}$ rated power of the fuel cell in [W], C_{BT} capacity of the battery bank 2 in [Wh], and C_{H2} the capacity of the hydrogen tank in [kg] of H2.

COEW	$\frac{E_{EXT}}{E_{Load}}$	$COEW_{max}$	$COEW_{min}$	$\left(\frac{E_{EXT}}{E_{Load}}\right)_{max}$	$\left(\frac{E_{EXT}}{E_{Load}}\right)_{min}$	C_{BT} [Wh]	C_{H2} [kg]	$P_{EL,rated}$ [W]	$P_{FC,rated}$ [W]
0.350	0.081	0.350	0.329	0.081	0.052	19924	203	40338	38780
0.351	0.079	0.351	0.329	0.079	0.051	20567	208	40840	39400

Table 11
Origins of sources of energy delivered to consumers (545 MWh)

	RES ↦ $Load_{electricity}$	RES ↦ $Load_{water}$	EXT	FC	BT-
Production in MWh	391.96	64.31	34.23	53.96	0.77
Distribution	71.92%	11.8%	6.28%	9.9%	0.14%

Table 12
Distribution of energy consumption from renewable sources (1090MWh)

	RES ↦ $Load_{electricity}$	RES ↦ $Load_{water}$	CURT	EL	BT+	Pure Water
Consumption or loss in MWh	391.96	64.31	414.96	217.34	1.3	0.1
Distribution	35.96%	5.90%	38.07%	19.94%	0.12%	0.01%

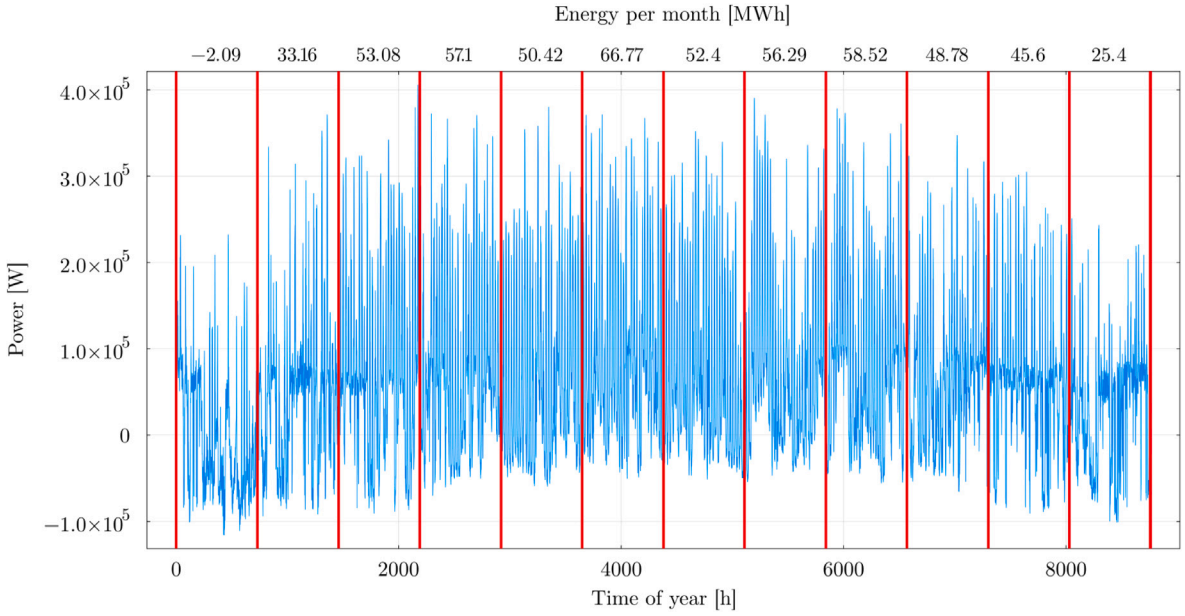

Fig. 20. Difference between renewable energy production and energy consumption (water + electricity) established hour by hour over the year of the dataset used (yL:2022/yR:2022).

minimize this energy loss without increasing the final cost of energy, for example, by increasing the size of the electrolyzer and hydrogen storage. It should be noted that without the storage system, the overall efficiency of the system would only be 35.96%. These results depend on the match between electricity needs that are difficult to predict and control and energy production that will depend on uncontrollable and hard-to-predict weather conditions.

If weather conditions cannot be controlled, surplus energy can be used to meet other needs which are more controllable than electrical needs. The original idea behind the C3POe project is to use this surplus to produce drinking water. This reduces electrical waste by 5.9%, in the studied case. Although water requirements are also difficult to predict and control, storing water is much easier than storing electricity. The originality of this article lies in its presentation of energy and water management system that reconciles the need for water and electricity. On the same principle, other controllable systems can be implemented as part of the energy management system, to recover surplus energy by producing co-products. Although beyond the scope of this article, this approach could make it possible to totally eliminate energy wastage, which in the case studied amounts to more than a third of the energy produced by renewables.

To ensure that EWMS is operating correctly, the levels have to be checked. As shown in Fig. 23, water production switches to priority when the low level $LOW1_{end,priority}$ is reached and stops when the $LOW2_{end,priority}$ level is reached. In the non-priority state, production benefits from excess energy to fill the water tank. Other priority rules for water can be defined to limit energy losses during periods of shortage. In the case studied, in winter (200–300 h), when the hydrogen reservoir has reached its minimum limit, the production of drinking water is a priority, so the system is obliged to produce energy from an external source. A larger quantity of water could have been produced in summer when the hydrogen tanks were full, to make up for the shortfall in winter. However, this would have required greater water storage capacity. By default, the size of the water tank was fixed in the sizing process, as it is not the responsibility of the C3POe consortium. Table 13 shows the elements used to calculate the lifetime of the various subsystems. On average, the electrolyzer has a continuous operating cycle of around 15 h, and the fuel cell a continuous operating cycle of around 6 h. A breakdown of costs is shown in Table 14. The particular point to note is that replacements make up 18% of the total cost and should not be neglected. The hydrogen chain (FC, ELY, H2 tank) accounts for 28% of total costs, and the two battery banks for 5%.

Table 13
Number of operating hours nb_h, number of on–offs I/O, and subsystem lifetime.

	nb_h	I/O	$Lifetime$[year]
EL	5047	340	9.22
FC	2006	315	10.16
RO1	5755	385	
RO2	72	72	

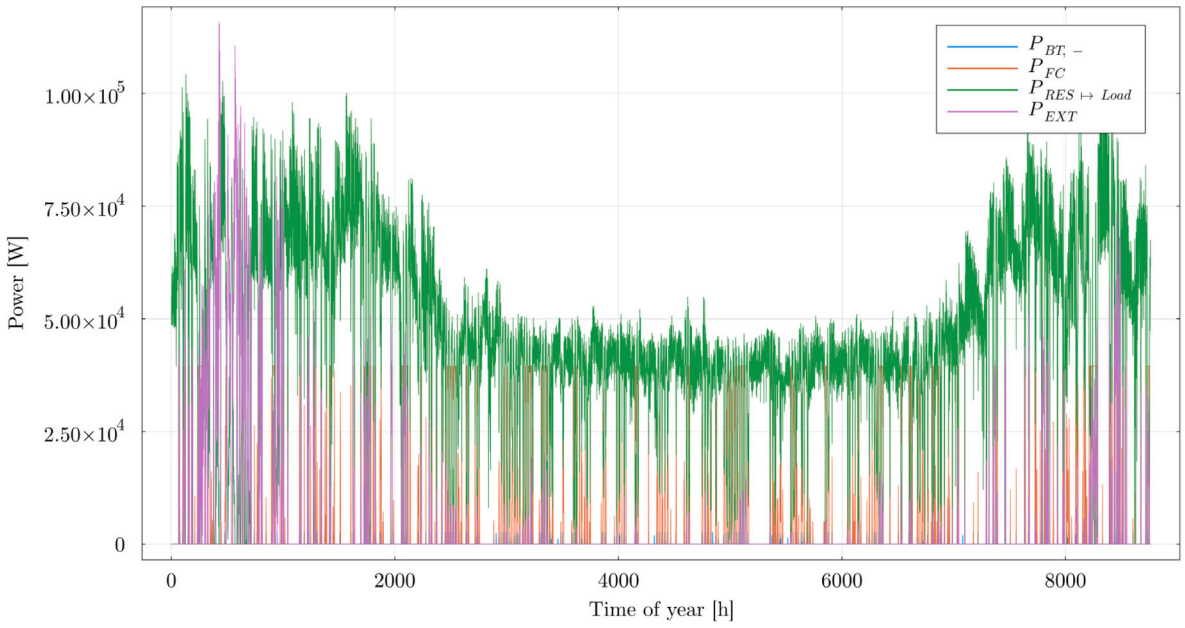

Fig. 21. Hour by hour energy production delivered to the consumer, $P_{BT,-}$: energy discharged from the battery, P_{FC}: energy supplied by the fuel cell, $P_{RES \mapsto Load}$: energy from renewable sources delivered directly to the consumer without passing through the C3POe system, P_{EXT}: energy supplied by a source external to the C3POe system.

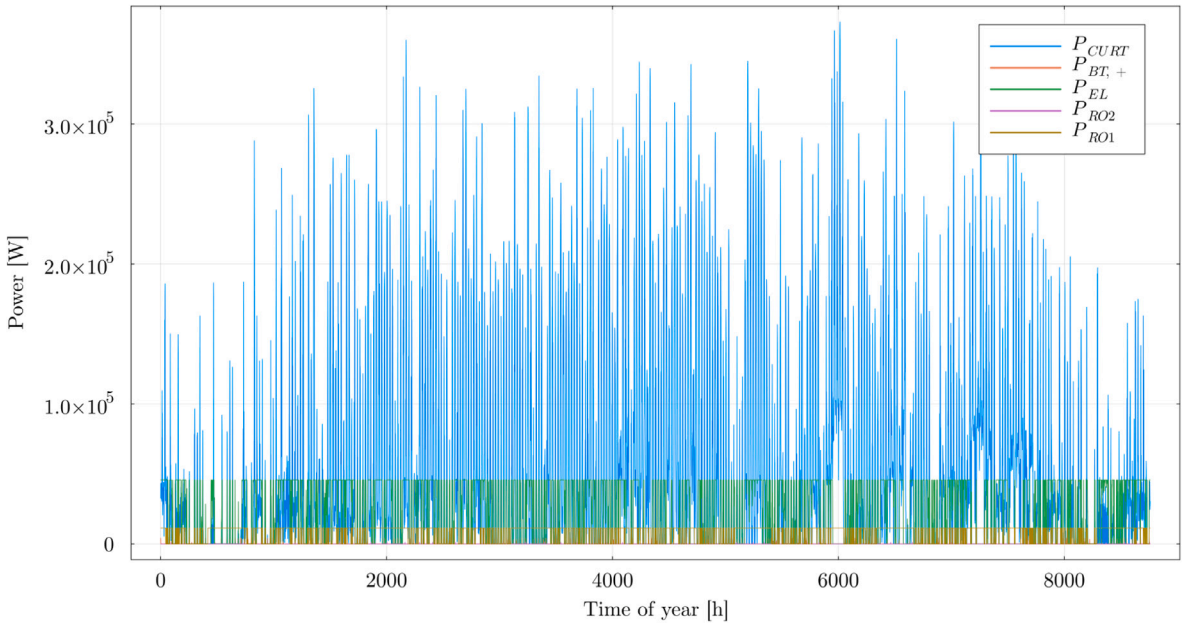

Fig. 22. Energy consumed hourly by the C3POe system or curtailed, P_{CURT}: curtailed energy, $P_{BT,-}$: energy charged in the battery, P_{EL}: energy consumed by the electrolyzer, P_{RO1}: energy consumed by reverse osmosis system 1, P_{RO2}: energy consumed by the reverse osmosis system 2.

Table 14
Cost partition.

C3POe			EXT	RES
inv	om	rep		
31%	8%	18%	5%	38%

7. Conclusion

In this study, a novel methodology was developed for the optimal sizing of hybrid renewable energy systems designed to supply both electricity and drinking water in off-grid contexts. The approach is based on Pareto front analysis and a newly introduced shortage indicator, allowing a robust assessment of system configurations under varying input conditions. A key innovation was the explicit incorporation of input data uncertainty — including meteorological and demand profiles — into the system design process. The shortage indicator proved effective in distinguishing favorable from unfavorable data conditions for a given photovoltaic-wind energy mix, providing a computationally efficient and operationally relevant tool.

The results shown in Figs. 14, 15, & 16, reveal a critical methodological pitfall that is often overlooked in comparable studies: for each scenario, the Pareto fronts significantly differ depending on whether favorable (low shortage indicator S) or unfavorable (high shortage indicator S) input datasets are used. Each front represents optimized

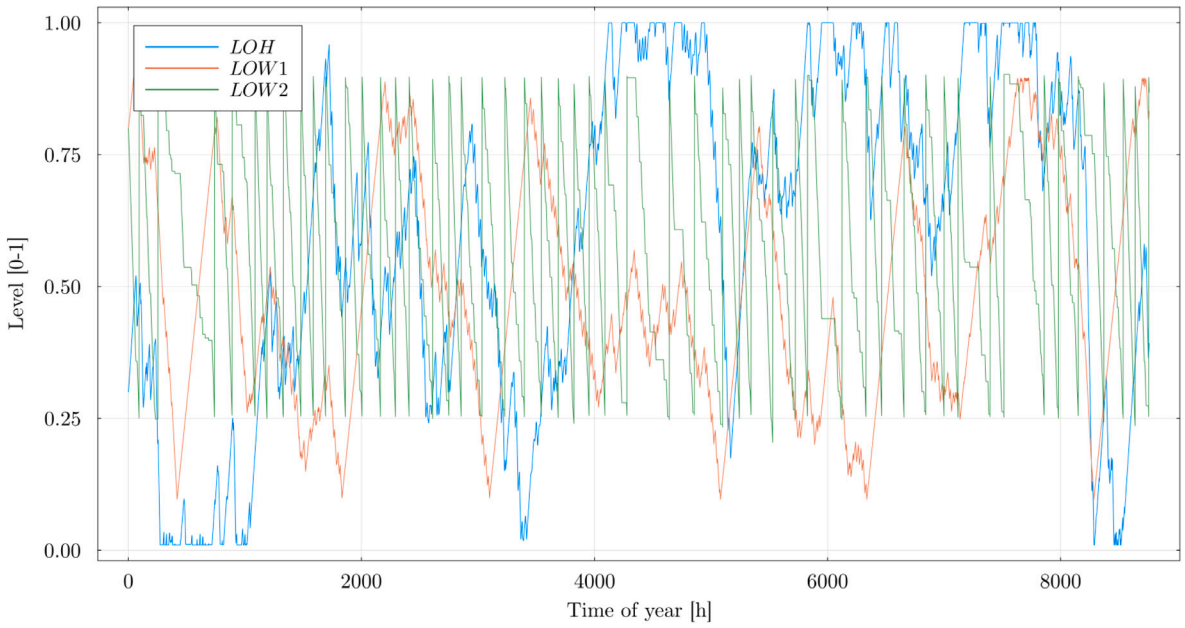

Fig. 23. Hour-by-hour changes of the levels of LOH:hydrogen, $LOW1$:drinking water and $LOW2$:pure water.

system configurations balancing cost ($COEW$) and renewable energy usage (E_{EXT}/E_{Load}). A decision-maker using a single input dataset to design the system would only obtain one Pareto front and could therefore be misled in selecting an optimal configuration. For instance, targeting a fixed energy cost, the system design may vary considerably depending on the input data, as evidenced by the differences in battery and hydrogen storage capacities in Tables 8 and 9.

This observation justifies the need for both a multi-objective optimization approach — considering cost and renewable share simultaneously — and a systematic exploration of the variability in input data (meteorological and consumption profiles). The shortage indicator S introduced in this work enables the identification of the most and least favorable datasets, thus limiting the number of required simulations while capturing the full range of system behaviors.

Neglecting either the multi-objective nature of the problem or the input variability leads to incomplete or potentially inaccurate system designs. This study demonstrates that the renewable share and system cost are deeply interdependent: improving one objective inevitably comes at the expense of the other. Therefore, decision-making must be based on a comprehensive analysis of Pareto fronts obtained under various input scenarios.

Looking forward, several avenues for future research are identified. More detailed physical models of key subsystems (electrolyzer, fuel cell, battery, and RO unit) could be incorporated to better reflect aging effects and dynamic behavior. In addition, substantial renewable energy surpluses were observed, which suggests the potential for integration of flexible, on-demand applications such as wastewater treatment, heat production, or desalination. A comprehensive sensitivity analysis is planned to assess the impact of modeling assumptions and further enhance the robustness of the methodology.

CRediT authorship contribution statement

Florent Struyven: Software, Formal analysis, Visualization, Investigation, Conceptualization, Writing – original draft, Methodology, Data curation. **Mathieu Sellier:** Supervision, Visualization, Writing – review & editing. **Myeongsub Kim:** Supervision, Visualization, Writing – review & editing. **Rosalinda Inguanta:** Supervision, Visualization, Writing – review & editing. **Farkad A. Lattieff:** Writing – review & editing, Supervision, Validation, Visualization. **Philippe Mandin:** Writing – review & editing, Supervision, Methodology, Formal analysis, Validation, Project administration, Funding acquisition, Conceptualization, Visualization, Resources, Investigation, Data curation.

Declaration of competing interest

The authors declare the following financial interests/personal relationships which may be considered as potential competing interests: Mandin Philippe reports financial support was provided by European funding FEDER. Mandin Philippe reports financial support was provided by Brittany Region. Mandin Philippe reports a relationship with ENTECH that includes: board membership and non-financial support. Mandin Philippe reports a relationship with H2X that includes: board membership and non-financial support. Mandin Philippe reports a relationship with SLCE that includes: board membership and non-financial support. Mandin reports financial support was provided by European Union. Mandin reports financial support was provided by Brittany Region. Mandin reports a relationship with ENTECH that includes: board membership, consulting or advisory, funding grants, non-financial support, paid expert testimony, speaking and lecture fees, and travel reimbursement. Mandin reports a relationship with H2X that includes: board membership, consulting or advisory, funding grants, non-financial support, paid expert testimony, speaking and lecture fees, and travel reimbursement. Mandin reports a relationship with SLCE that includes: board membership, consulting or advisory, funding grants, non-financial support, paid expert testimony, speaking and lecture fees, and travel reimbursement. The Corresponding author, Pr. Philippe Mandin, is in charge for South Brittany University & for IRDL UMR CNRS 6027 of the C3POe funded project. He is in charge naely of this project, its results for partners ENETCH, H2X and SLCE. He is in charge of all energy and electrochemistry engineering, mainly for batteries and hydrogen engineering, for his university UBS and his lab IRDL UMR CNRS 6027. If there are other authors, they declare that they have no known competing financial interests or personal relationships that could have appeared to influence the work reported in this paper. If there are other authors, they declare that they have no known competing financial interests or personal relationships that could have appeared to influence the work reported in this paper. If there are other authors, they declare that they have no known

competing financial interests or personal relationships that could have appeared to influence the work reported in this paper.

Acknowledgments

The endeavors undertaken in this project were conducted within the framework of the C-3POe initiative, with co-funding provided by the FEDER, European Regional Development Fund, the Brittany Regional Council, France, Lorient Agglomération, and Rennes Métropole, for which we are deeply grateful for their financial support. Additionally, we extend our heartfelt appreciation to our esteemed collaborative partners - ENTECH, H2X ECOSYSTEM, SLCE and Moulins Bleus - for their invaluable collaboration.

References

[1] IRENA. Off-grid renewable energy systems: Status and methodological issues. 2015.
[2] Blechinger P, Cader C, Bertheau P, Huyskens H, Seguin R, Breyer C. Global analysis of the techno-economic potential of renewable energy hybrid systems on small islands. Energy Policy 2016;98:674–87.
[3] Groppi D, Astiaso Garcia D, Lo Basso G, Cumo F, De Santoli L. Analysing economic and environmental sustainability related to the use of battery and hydrogen energy storages for increasing the energy independence of small islands. Energy Convers Manage 2018;177:64–76.
[4] Marocco P, Ferrero D, Gandiglio M, Ortiz M, Sundseth K, Lanzini A, et al. A study of the techno-economic feasibility of H2-based energy storage systems in remote areas. Energy Convers Manage 2020;211:112768.
[5] Cai W, Li X, Maleki A, Pourfayaz F, Rosen MA, Alhuyi Nazari M, et al. Optimal sizing and location based on economic parameters for an off-grid application of a hybrid system with photovoltaic, battery and diesel technology. Energy 2020;201:117480.
[6] Jamshidi M, Askarzadeh A. Techno-economic analysis and size optimization of an off-grid hybrid photovoltaic, fuel cell and diesel generator system. Sustain Cities Soc 2019;44:310–20.
[7] Lund H, Sorknæ s P, Mathiesen BV, Hansen K. Beyond sensitivity analysis: A methodology to handle fuel and electricity prices when designing energy scenarios. Energy Res Soc Sci 2018;39:108–16.
[8] International Energy Agency. World energy outlook 2023. Technical report, International Energy Agency; 2023.
[9] Marocco P, Ferrero D, Lanzini A, Santarelli M. Optimal design of stand-alone solutions based on RES + hydrogen storage feeding off-grid communities. Energy Convers Manage 2021;238:114147.
[10] UNFCC. Paris agreement. 2015.
[11] Larch M, Wanner J. The consequences of non-participation in the Paris Agreement. Eur Econ Rev 2024;163:104699.
[12] Alessi L, Battiston S, Kvedaras V. Over with carbon? Investors' reaction to the Paris Agreement and the US withdrawal. J Financ Stab 2024;71:101232.
[13] IRENA I. Global renewables outlook: Energy transformation 2050. Technical report, 2020.
[14] Olabi A, Onumaegbu C, Wilberforce T, Ramadan M, Abdelkareem MA, Al Alami AH. Critical review of energy storage systems. Energy 2021;214:118987.
[15] Wali SB, Hannan M, Reza M, Ker PJ, Begum R, Rahman MA, et al. Battery storage systems integrated renewable energy sources: A biblio metric analysis towards future directions. J Energy Storage 2021;35:102296.
[16] Blanco H, Faaij A. A review at the role of storage in energy systems with a focus on Power to Gas and long-term storage. Renew Sustain Energy Rev 2018;81:1049–86.
[17] Buffo G, Marocco P, Ferrero D, Lanzini A, Santarelli M. Power-to-x and power-to-power routes. In: Solar hydrogen production. Elsevier; 2019, p. 529–57.
[18] International Energy Agency. The Future of Hydrogen License: CC BY 4.0. Technical report, International Energy Agency; 2019.
[19] FCH. Hydrogen Roadmap Europe. Technical report, European community; 2019.
[20] IRENA E. Global Hydrogen Trade to Meet the 1.5° C Climate Goal: Part III—Green Hydrogen Cost and Potential. united arab emirates: International renewable energy agency abu dhabi; 2022.
[21] Nordin ND, Rahman HA. Comparison of optimum design, sizing, and economic analysis of standalone photovoltaic/battery without and with hydrogen production systems. Renew Energy 2019;141:107–23.
[22] Ozden E, Tari I. PEM fuel cell degradation effects on the performance of a stand-alone solar energy system. Int J Hydrog Energy 2017;42(18):13217–25.
[23] Chiron T. Quelle gestion durable des ressources en eau et du risque de penurie sur les petites îles? (Ph.D. thesis), Université de Bretagne occidentale-Brest; 2007.
[24] Lian J, Zhang Y, Ma C, Yang Y, Chaima E. A review on recent sizing methodologies of hybrid renewable energy systems. Energy Convers Manage 2019;199:112027.
[25] Maleki A, Askarzadeh A. Comparative study of artificial intelligence techniques for sizing of a hydrogen-based stand-alone photovoltaic/wind hybrid system. Int J Hydrog Energy 2014;39(19):9973–84.
[26] Jallouli R, Krichen L. Sizing, techno-economic and generation management analysis of a stand alone photovoltaic power unit including storage devices. Energy 2012;40(1):196–209.
[27] Javed MS, Jurasz J, Guezgouz M, Canales FA, Ruggles TH, Ma T. Impact of multi-annual renewable energy variability on the optimal sizing of off-grid systems. Renew Sustain Energy Rev 2023;183:113514.
[28] Karavas C-S, Arvanitis KG, Papadakis G. Optimal technical and economic configuration of photovoltaic powered reverse osmosis desalination systems operating in autonomous mode. Desalination 2019;466:97–106.
[29] Nguyen HT, Safder U, Nhu Nguyen X, Yoo C. Multi-objective decision-making and optimal sizing of a hybrid renewable energy system to meet the dynamic energy demands of a wastewater treatment plant. Energy 2020;191:116570.
[30] Rullo P, Braccia L, Luppi P, Zumoffen D, Feroldi D. Integration of sizing and energy management based on economic predictive control for standalone hybrid renewable energy systems. Renew Energy 2019;140:436–51.
[31] Mandelli S, Brivio C, Colombo E, Merlo M. Effect of load profile uncertainty on the optimum sizing of off-grid PV systems for rural electrification. Sustain Energy Technol Assess 2016;18:34–47.
[32] Burgio A, Menniti D, Sorrentino N, Pinnarelli A, Leonowicz Z. Influence and Impact of Data Averaging and Temporal Resolution on the Assessment of Energetic, Economic and Technical Issues of Hybrid Photovoltaic-Battery Systems. Energies 2020;13(2):354.
[33] Stenzel P, Linssen J, Fleer J, Busch F. Impact of temporal resolution of supply and demand profiles on the design of photovoltaic battery systems for increased self-consumption. In: 2016 IEEE international energy conference (ENERGYCON). Leuven, Belgium: IEEE; 2016, p. 1–6.
[34] Olatomiwa L, Mekhilef S, Ismail MS, Moghavvemi M. Energy management strategies in hybrid renewable energy systems: A review. Renew Sustain Energy Rev 2016;62:821–35.
[35] Vivas FJ, De las Heras A, Segura F, Andújar JM. A review of energy management strategies for renewable hybrid energy systems with hydrogen backup. Renew Sustain Energy Rev 2018;82:126–55.
[36] Ulleberg O. The importance of control strategies in PV–hydrogen systems. Sol Energy 2004;76(1):323–9.
[37] Zhou K, Ferreira JA, de Haan SWH. Optimal energy management strategy and system sizing method for stand-alone photovoltaic-hydrogen systems. Int J Hydrog Energy 2008;33(2):477–89.
[38] Jyoti Saharia B, Brahma H, Sarmah N. A review of algorithms for control and optimization for energy management of hybrid renewable energy systems. J Renew Sustain Energy 2018;10(5):053502.
[39] Salehi N, Martinez-Garcia H, Velasco-Quesada G, Guerrero JM. A Comprehensive Review of Control Strategies and Optimization Methods for Individual and Community Microgrids. IEEE Access 2022;10:15935–55.
[40] Oyewole OL, Nwulu NI, Okampo EJ. Optimal design of hydrogen-based storage with a hybrid renewable energy system considering economic and environmental uncertainties. Energy Convers Manage 2024;300:117991.
[41] National Renewable Energy Laboratory. Golden, CO..PySAM version 4.2.0. 2024.
[42] Li B, Roche R, Paire D, Miraoui A. Sizing of a stand-alone microgrid considering electric power, cooling/heating, hydrogen loads and hydrogen storage degradation. Appl Energy 2017;205:1244–59.
[43] Le TS, Nguyen TN, Bui D-K, Ngo TD. Optimal sizing of renewable energy storage: A techno-economic analysis of hydrogen, battery and hybrid systems considering degradation and seasonal storage. Appl Energy 2023;336:120817.
[44] Ozden E, Tari I. Proton exchange membrane fuel cell degradation: A parametric analysis using Computational Fluid Dynamics. J Power Sources 2016;304:64–73.
[45] Pei P, Chen H. Main factors affecting the lifetime of Proton Exchange Membrane fuel cells in vehicle applications: A review. Appl Energy 2014;125:60–75.
[46] El-kharouf A, Chandan A, Hattenberger M, Pollet BG. Proton exchange membrane fuel cell degradation and testing: review. J Energy Inst 2012;85(4):188–200, Publisher: Taylor & Francis _eprint: https://www.tandfonline.com/doi/pdf/10.1179/1743967112Z.00000000036.
[47] Yu Y, Li H, Wang H, Yuan X-Z, Wang G, Pan M. A review on performance degradation of proton exchange membrane fuel cells during startup and shutdown processes: Causes, consequences, and mitigation strategies. J Power Sources 2012;205:10–23.
[48] Hua Z, Zheng Z, Pahon E, Péra M-C, Gao F. A review on lifetime prediction of proton exchange membrane fuel cells system. J Power Sources 2022;529:231256.
[49] Brissaud F, Chaise A, Gault K, Soual S. Lessons learned from Jupiter 1000, an industrial demonstrator of Power-to-Gas. Int J Hydrog Energy 2024;49:925–32.
[50] Buttler A, Spliethoff H. Current status of water electrolysis for energy storage, grid balancing and sector coupling via power-to-gas and power-to-liquids: A review. Renew Sustain Energy Rev 2018;82:2440–54.
[51] Ozturk M, Dincer I. A comprehensive review on power-to-gas with hydrogen options for cleaner applications. Int J Hydrog Energy 2021;46(62):31511–22.
[52] Li B, Roche R, Miraoui A. Microgrid sizing with combined evolutionary algorithm and MILP unit commitment. Appl Energy 2017;188:547–62.
[53] Santos M, Marino I. Energy analysis of the Raggovidda integrated system. Tech rep, 779469, 2019.

[54] Brauns J, Turek T. Alkaline Water Electrolysis Powered by Renewable Energy: A Review. Processes 2020;8(2):248, Number: 2 Publisher: Multidisciplinary Digital Publishing Institute.
[55] Torreglosa JP, García-Triviño P, Fernández-Ramirez LM, Jurado F. Control based on techno-economic optimization of renewable hybrid energy system for stand-alone applications. Expert Syst Appl 2016;51:59–75.
[56] Bordin C, Anuta HO, Crossland A, Gutierrez IL, Dent CJ, Vigo D. A linear programming approach for battery degradation analysis and optimization in offgrid power systems with solar energy integration. Renew Energy 2017;101:417–30, Publisher: Elsevier.
[57] Colla M, Ioannou A, Falcone G. Critical review of competitiveness indicators for energy projects. Renew Sustain Energy Rev 2020;125:109794.
[58] Kuckshinrichs W. LCOE: A Useful and Valid Indicator—Replica to James Loewen and Adam Szymanski. Energies 2021;14(2):406, Number: 2 Publisher: Multidisciplinary Digital Publishing Institute.
[59] Loewen J. LCOE is an undiscounted metric that inaccurately disfavors renewable energy resources. Electr J 2020;33(6):106769.
[60] Loewen J. LCOE is an undiscounted metric that distorts comparative analyses of energy costs. Electr J 2019;32(6):40–2.
[61] Ueckerdt F, Hirth L, Luderer G, Edenhofer O. System LCOE: What are the costs of variable renewables? Energy 2013;63:61–75.
[62] Hadka D, Reed P. Diagnostic assessment of search controls and failure modes in many-objective evolutionary optimization. Evol Comput 2012;20(3):423–52.
[63] Hadka D, Reed P. Borg: An auto-adaptive many-objective evolutionary computing framework. Evol Comput 2013;21(2):231–59.
[64] Hadka D, Reed P. Large-scale parallelization of the borg multiobjective evolutionary algorithm to enhance the management of complex environmental systems. Environ Model Softw 2014.
[65] Hadka D, Madduri K, Reed P. Scalability analysis of the asynchronous master-slave borg multiobjective evolutionary algorithm. In: The 16th international workshop on nature inspired distributed computing (NIDISC) at the 27th IEEE/ACM international parallel and distributed processing symposium. Boston, MA; 2013.
[66] Hadka D, Reed P, Simpson T. Diagnostic assessment of the borg MOEA for many-objective product family design problems. In: WCCI 2012 world congress on computational intelligence, congress on evolutionary computation. Brisbane, Australia; 2012, p. 986–95.